

# Core evidence of paleoseismic events in Paleogene deposits of the Shulu Sag in the Bohai Bay Basin, east China, and their petroleum geologic significance



Lijing Zheng <sup>a,b</sup>, Zaixing Jiang <sup>a,b,\*</sup>, Hui Liu <sup>c</sup>, Xiangxin Kong <sup>a</sup>, Haipeng Li <sup>a</sup>, Xiaolong Jiang <sup>d</sup>

<sup>a</sup> College of Energy, China University of Geosciences, Xueyuan Road, Haidian District, Beijing 100083, China

<sup>b</sup> Institute of Earth Sciences, China University of Geosciences, Beijing 100083, China

<sup>c</sup> Oil & Gas Survey, China Geological Survey, Anwai Road, Chaoyang District, Beijing 100029, China

<sup>d</sup> School of Earth and Mineral Sciences, The Pennsylvania State University, 201 Old Main, University Park, PA 16802, United States

## ARTICLE INFO

### Article history:

Received 10 March 2015

Received in revised form 27 July 2015

Accepted 27 July 2015

Available online 14 August 2015

Editor: B. Jones

### Keywords:

Seismites

Cores

Deformation structures

Seismoturbidites

Oil occurrence

East China

## ABSTRACT

The Shulu Sag, located in the southwestern corner of the Jizhong Depression, Bohai Bay Basin of east China, is a NE–SW trending, elongate Cenozoic half-graben basin. The lowermost part of the third member of the Shahejie Formation in this basin is characterized by continental rudstone and calcilutite to calcisiltite facies. Based on core observation and regional geologic analysis, seismites are recognized in these lacustrine deposits, which include soft-sediment deformation structures (sedimentary dikes, hydraulic shattering, diapir structures, convolute lamination, load-flame structures, ball-and-pillow structures, loop bedding, and subsidence structures), synsedimentary faults, and seismoturbidites. In addition, mixed-source rudstones, consisting of the Paleozoic carbonate clasts and *in situ* calcilutite clasts in the lowermost submember of Shahejie 3, appear in the seismites, suggesting an earthquake origin. A complete representative vertical sequence in the lowermost part of the third member found in well ST1H located in the central part of the Shulu Sag shows, from the base to the top: underlying undeformed layers, synsedimentary faults, liquefied carbonate rocks, alloogenetic seismoturbidites, and overlying undeformed layers. Seismites are widely distributed around this well and there are multiple sets of stacked seismites separated by undeformed sediment. The nearby NW-trending Taijiazhuang fault whose fault growth index is from 1.1 to 1.8 and the NNE-trending Xinhe fault with a fault growth index of 1.3–1.9 may be the source of the instability to create the seismites. These deformed sedimentary layers are favorable for the accumulation of oil and gas; for example, sedimentary dikes can cut through many layers and serve as conduits for fluid migration. Sedimentary faults and fractures induced by earthquakes can act as oil and gas migration channels or store petroleum products as well. Seismoturbidites and mixed-source rudstones are excellent reservoirs due to their abundant primary or dissolved pores.

© 2015 Elsevier B.V. All rights reserved.

## 1. Introduction

Synsedimentary deformation induced by earthquakes, referred to as “seismites,” increasingly attracts the attention of sedimentologists (e.g., El Taki and Pratt, 2012). Different types of seismites were produced through simulation experiments to assess the trigger mechanism and the processes that form soft-sediment deformation structures (SSDSs) (e.g., McKee and Goldberg, 1969; Nichols et al., 1994; Owen, 1996; Moretti et al., 1999). The valid criteria for identifying a seismic trigger include: ① deformation occurring in laterally extensive, recurring horizons, ② morphology comparable with structures described from earthquake, ③ a tectonically active basin, and ④ zonation of

complexity of deformation (Owen et al., 2011). The recognition of triggers for SSDSs plays a guiding role for the accurate identification of seismites (Owen and Moretti, 2011; Owen et al., 2011), although the criteria for recognition of seismites have not been widely accepted (Jones and Omoto, 2000; Montenat et al., 2007; Wallace and Eyles, 2015), depending on interpretations of deformation structures and geologic context.

Different types of seismites are well developed within fluvial (Guiraud and Plaziat, 1993; Mugnier et al., 2011; Santos et al., 2012), lacustrine (Sims, 1975; Rodríguez-Pascua et al., 2000; Bowman et al., 2004; Moretti and Sabato, 2007; Singh and Jain, 2007; Fortuin and Dabrio, 2008), and marine (Pratt, 2001; Qiao et al., 2007; Martín-Chivelet et al., 2011) deposits in outcrop where many phenomena on a large scale can be easily observed, such as lateral facies changes, large-scale sedimentary features, and macrofossils (Selley, 1978; Ethridge, 1993). By contrast, there are quite a number of limitations in studying seismites through

\* Corresponding author at: College of Energy, China University of Geosciences (Beijing), #29 Xueyuan Road, Beijing 100083, China.

E-mail address: [jiangzx@cugb.edu.cn](mailto:jiangzx@cugb.edu.cn) (Z. Jiang).

core observation because the cores' diameter is only approximately 10 cm. Considerable information loss also occurs if cores are mishandled (Siemers and Tillman, 1981). However, these disadvantages can be offset by the advantages of continuous cores, including fresh unweathered rock and a more complete section of the stratigraphic units and their fossils (Selleby, 1978; Siemers and Tillman, 1981; Ethridge, 1993). Most of the sediments containing SSDSs are documented in well cores as resedimentation events, such as homogenites (Chapron et al., 1999), seismoturbidites (Doig, 1986, 1990; Gorsline et al., 2000; Nakajima and Kanai, 2000; Wagner et al., 2008; Goldfinger, 2009, 2011; Leroy et al., 2010; Faridfathi and Ergin, 2012; Gutiérrez-Pastor et al., 2013), or flood event deposits (Arnaud et al., 2002). Nevertheless, there are few papers that interpret SSDSs as seismites in well cores (El Taki and Pratt, 2012; He et al., 2014; Ezquerro et al., 2015).

In this paper, seismites of Paleogene age in cores are described from the Shulu Sag of the Bohai Bay Basin of east China. The typical characteristic structures of seismic activity on unconsolidated sediments comprise widespread ball-and-pillow structures, hydraulic shattering, diapir structures, loop bedding, etc. This research on seismites focuses on description of SSDs in well cores, deformation processes and mechanisms (Allen, 1977; Owen, 1987; Rodríguez-Pascua et al., 2000; Moretti, 2000; Neuwerth et al., 2006; Rana et al., 2013; Ezquerro et al., 2015) and relationships with hydrocarbon reservoirs (He et al., 2014). The role of SSDSs (ductile and brittle deformation), seismoturbidites, and mixed-source rudstone as a fundamental trigger for porosity variations and oil occurrence is explored here.

## 2. Geologic setting

The Shulu Sag is located in the southwest area of the Jizhong Depression of the Bohai Bay Basin of east China (Fig. 1). It is a NE–SW trending half-graben covering 300 km<sup>2</sup>, whose east side is defined by the Xinhe fault and the west side overlaps the Ningjin uplift (Fig. 2A) (Jiang et al., 2007). Another set of nearly W–E to WNW–ESE-trending faults was formed during the Middle Jurassic to Late Cretaceous Yanshanian Orogeny (Yang et al., 2001), namely the Hengshui, Taijiazhuang, and Jinqiu faults (Fig. 2B). These preexisting faults control the topographic relief within the basin, and divide the basin into three parts: the northern, middle, and southern (Jiang et al., 2007; Zhao et al., 2014). The study area is located in the middle portion of this basin surrounding the town of Checheng.

The basement rocks of the Shulu Sag are composed of Archean–Paleoproterozoic metamorphic rocks and Meso-Neoproterozoic through Paleozoic sedimentary strata (Jiang et al., 2007; Zhao et al., 2014), consisting of Cambro-Ordovician and Permo-Carboniferous strata, including limestones and dolostones, directly overlain by Paleogene lacustrine basin fill (Zhao et al., 2014). There are five formations in the basin fill from top to bottom: the Pingyuan, Minghuazhen, Guantao, Dongying, and Shahejie Formations (Fig. 2C). The Shahejie Formation can be further split into three members: No. 1 (Es1), No. 2 (Es2), and No. 3 (Es3); the Shahejie 3 or Es3 consists of three submembers, the lower, middle, and upper. The upper submember is characterized by dark-gray mudstones interbedded with fine-grained sandstones (Jiang et al., 2007). The middle submember consists of argillaceous limestone

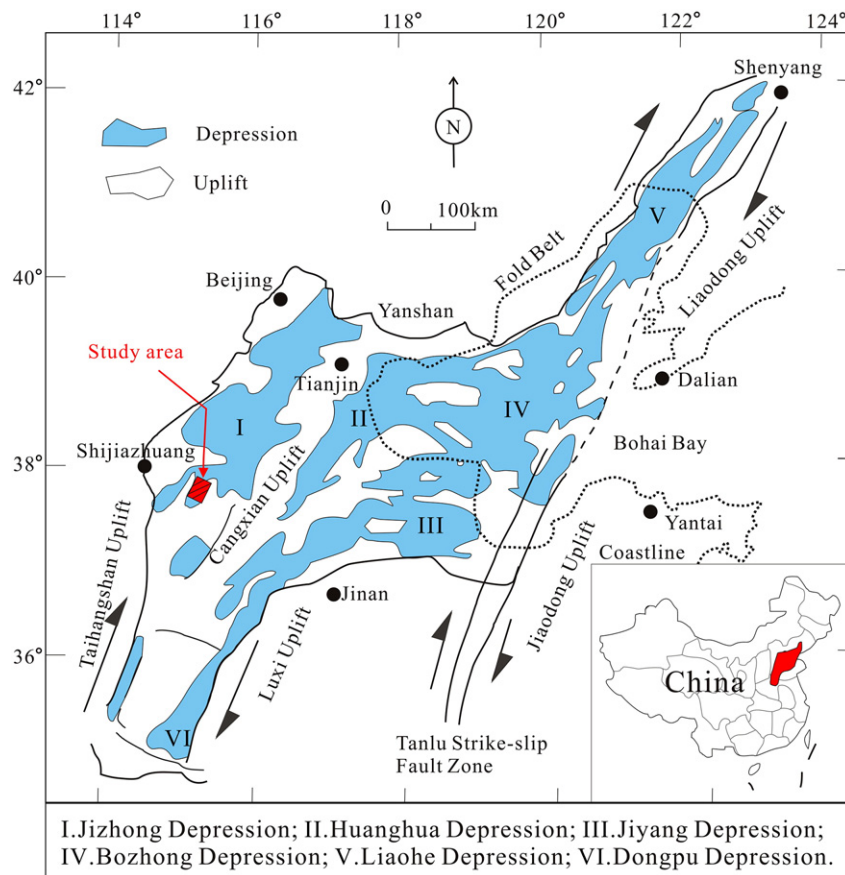


**Fig. 1.** Tectonic setting of the Paleogene Shulu Sag, located in the southwestern corner of the Jizhong Depression (I) of the Bohai Bay Basin of east China, which is composed of six sub-basins, named as depressions I–VI.  
After Jiang et al. (2007).

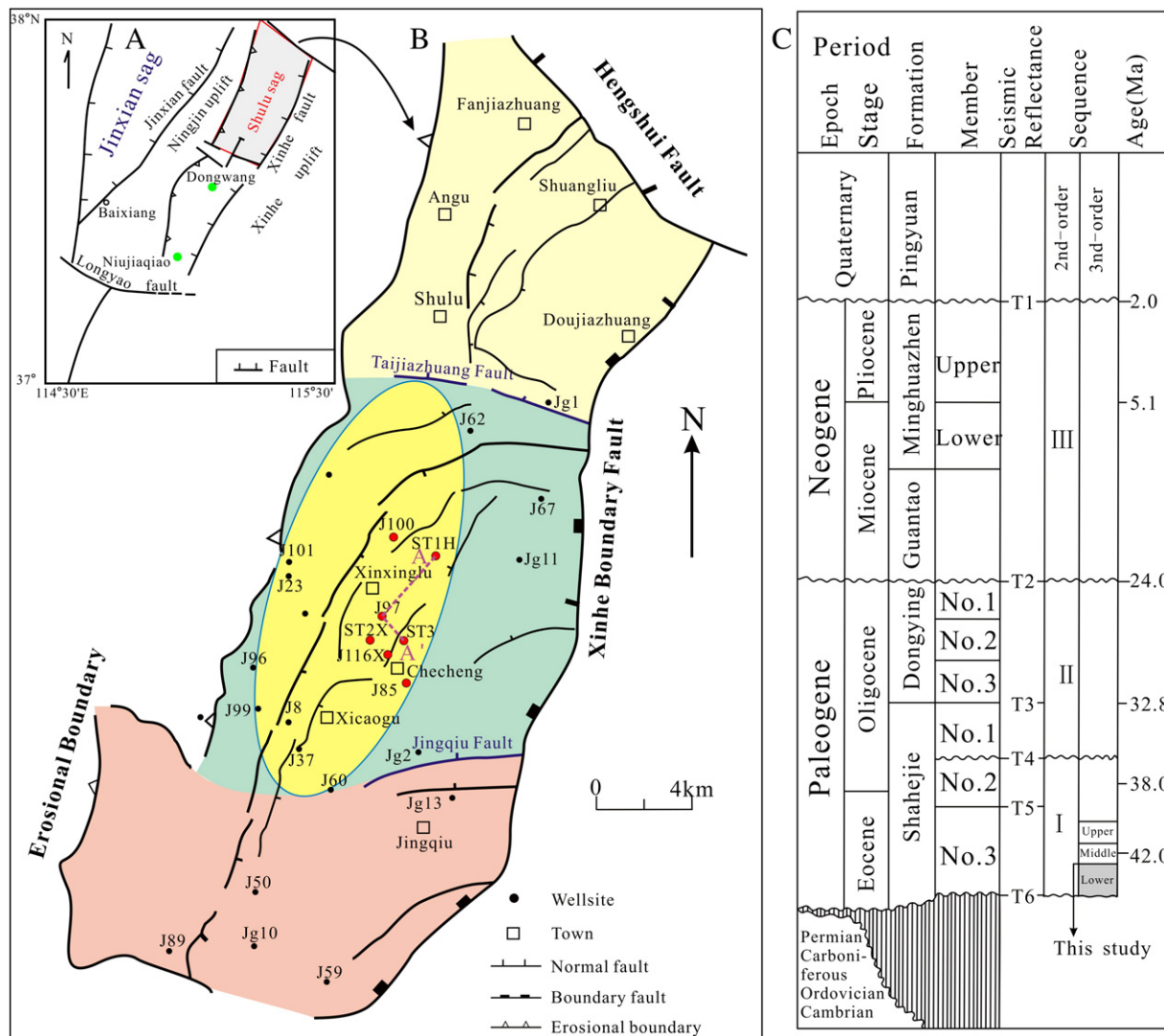


**Fig. 2.** (A) Geologic setting of the Shulu Sag half-graben. (B) Structural map of the Shulu half-graben. Three segments are delimited by the Taijiazhuang and Jingqiu faults. Wells are located by dots with their designations. Soft-sediment deformation is found in the wells located with red dots. Section A–A' in the yellow area is the location of Fig. 17. (C) Stratigraphic framework of the Shulu Sag.

(B) Modified after Jiang et al. (2007) and Wang et al. (1994). (C) The age data are derived from Ye et al. (1993).

(or marlstones) intercalated with shales. The lowermost submember of the Shahejie 3 contains carbonate breccia and calcilutite, which is the focus of this study. The maximum thickness of the target stratum is up to 1200 m in the basin depocenter and can be divided into five sequences: I, II, III, IV, and V (Fig. 3).

The Paleogene lake basin received both clastic carbonate bedload and carbonates dissolved in solution as suspended load, both brought by rivers or floods (after Gierlowski-Kordesch, 1998, 2010). The carbonate sedimentary rocks of the Shulu Sag were derived from the east, south, and west of the sag where the Phanerozoic carbonates are exposed as provenance. Lithofacies in the Shulu Sag contain clast-supported rudstone, matrix-supported rudstone, mixed-source rudstone, interlaminated calcisiltite–calcareous, calcarenous, laminated calcilutite, and massive calcilutite (Fig. 3). Based on sedimentary features and depositional geometries, most of lithofacies of the Shulu Sag represent lacustrine profundal to fan-delta sedimentation in each of the five sequences, portions of which are disturbed by SSDSs. The clast-supported rudstone, matrix-supported rudstone, and calcarenous on the western gentle slope edge of the basin are interpreted as deposits formed in the fan-delta plain and delta front. Most of them are structureless, and normal graded beds are rare in general. The sedimentary rocks near

the Xinhe fault are interpreted as lacustrine deep fan deposits, but few cores are available from this area. Uniquely, in Sequence III there are extensive autochthonous soft-sediment deformation containing sedimentary dikes, convolute lamination, and synsedimentary faults located around well ST1H (for location, see Fig. 2B). A unit of clast-supported rudstone, nearly 100 m thick, is also in this sequence and it is poorly sorted with massive and graded bedding. Mixed-source rudstone units, several meters in thickness, are relatively common. They comprise Paleozoic carbonate rocks transported from the Ningjin uplift and Paleogene intrabasin gravel-sized micritic intraclasts with deformational characteristics of soft sediment. Thick clast-supported rudstone and mixed-source rudstone are the main lithology of interpreted debris flows.

Although the laminated calcilutite and massive calcilutite are both dark-colored, the former contains regular to irregular, continuous to discontinuous laminae and the latter has no sedimentary structures. Interlaminated calcisiltite–calcareous is composed of thin dark calcilutite and tan calcarenous. No bedload sedimentary structures are present in the cores of these fine-grained sedimentary rocks and they are interpreted as profundal deposits.

The evolution of each sedimentary system is controlled by tectonism, paleotopography, provenance, and paleoclimate (Jiang et al., 2007). All of

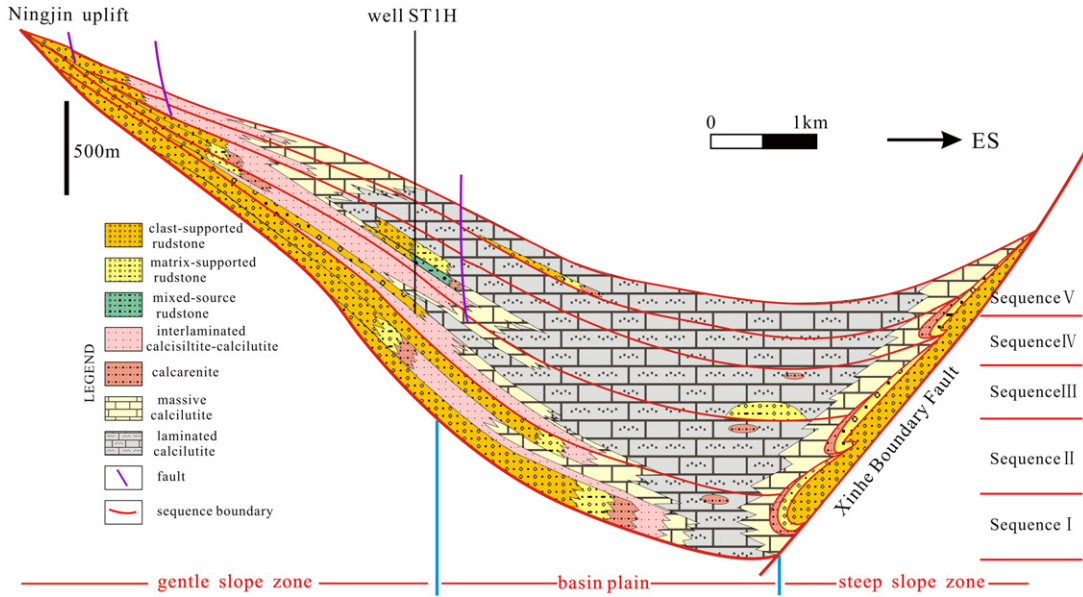


**Fig. 3.** Sketch of a transverse section through well ST1H in the lowermost submember of Es3 of the Shulu Sag. According to the 3D seismic and borehole data, the formation can be divided into five sequences: I, II, III, IV, and V, from bottom to top.

the terrigenous clasts of gray in color are derived from the Paleozoic carbonate rocks in the Ningjin uplift, including micrite, dolomitic, crystalline dolomite, silicified limestone, oolitic limestone, bioclastic limestone, pelleted limestone, and flat-pebble rudstone.

In this study, approximately 400 m of cores from 12 wells from Sequence I through V was carefully measured and described. The cores located in Sequence III are the longest, up to 156 m, followed in length by Sequence II and Sequence V. The cores located in Sequence IV are the shortest, only 12 m in length. During deposition of the Shahejie 3 member, the NW-trending Taijiazhuang fault growth index was from 1.1 to 1.8 and the NNE-trending Xinhe fault growth index was 1.3–1.9 (Kong et al., 2005). Some synsedimentary faults developed along the western slope of the depression, showing consequent normal faulting along a NE trending zone (Fig. 2B). These active tectonic zones provided the necessary conditions for forming seismites and may be the seismogenic structures creating the SSDSs.

### 3. Sedimentary features of the deformation structures

Many kinds of soft-sediment deformation are present in the lowermost submember of Shahejie 3 in the cores drilled in the central portion of the Shulu Sag of the Jizhong Depression within the Bohai Bay Basin of east China, such as sedimentary dikes, load-flame structures, and loop bedding. Seismic events may cause liquefaction and collapsing of huge volumes of sediments on the basin margins (Montenat et al., 2007). Liquefaction refers to the process by which water-saturated, unconsolidated sediments are transformed into a substance that behaves like a liquid due to loss of shear strength. Other deformation features during earthquakes include compression, shearing, extension, and dewatering (e.g., El Taki and Pratt, 2012). Effects of seismic shaking on sediments may be classified into three main categories (Fig. 4) (Montenat et al., 2007; Qiao and Li, 2009). The first category includes (1) soft-sediment liquefaction caused by shaking and an increase in pore pressure, such

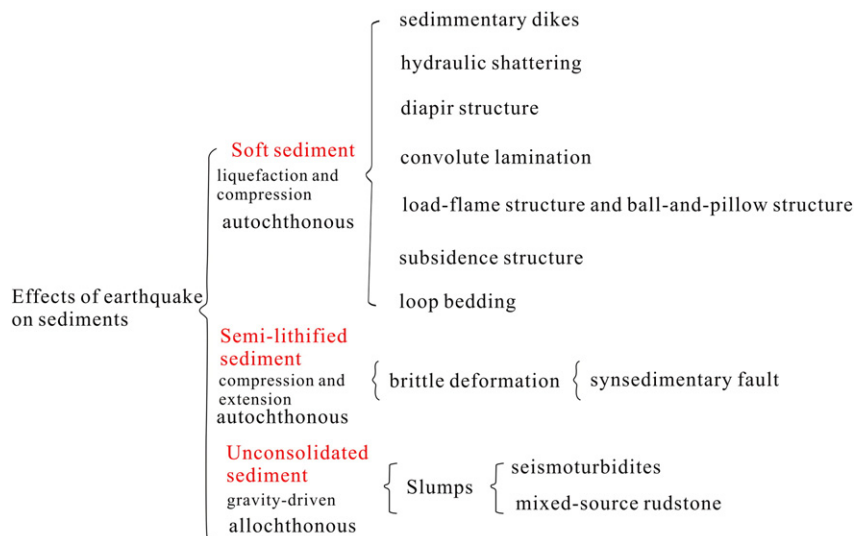


**Fig. 4.** Types of seismites in the Shulu Sag.  
After Montenat et al. (2007) and Qiao and Li (2009).

as diapirs and (2) deformation affected by episodic stress with minimal liquefaction, including loop bedding. The second category involves brittle deformation, such as synsedimentary faults. The third category refers to sediment deposits that move due to gravity-driven slumping, such as debris flows, mudflows, or turbidites. Different types of SSDSs are widely distributed in the cores of the Shulu Sag and are discussed in the following section.

### 3.1. Soft-sediment deformation

#### 3.1.1. Sedimentary dikes

**3.1.1.1. Description.** Sedimentary dikes are common in Sequence III. They consist typically of soft-sediment injections that crosscut laminated strata. The infill varies in color from faint yellow to gray, and in grain size from coarse-grained silt to fine gravel. They may be called clay dikes, sand dikes, breccia dikes, or carbonate micrite veins. The clastic dikes exhibit irregular morphologies and terminate downward, straight to sinuous in vertical view. Thickness of dikes constantly changes and the shape of these liquefied bodies can be enteroid, conical, or tabular. Dikes may exceed 10 cm in vertical extent (Fig. 5A) and are up to 3 cm wide. At their termination, dikes are thinner with a detached calcarenite nodule. Two breccia dikes can merge into one and end with a recumbent tail (Fig. 5B). Gravel-sized clasts associated with these dikes are poorly sorted, sub-rounded, or subangular. In well ST2X (for location, see Fig. 2B), calcarenite dikes taper downward and branch and two of the branches can be cut into three parts by microfaults (Fig. 5C and D).

**3.1.1.2. Interpretation.** Sedimentary dikes are penecontemporaneous with sedimentation (Martel and Gibling, 1993). They are formed by the injection of fluidized sediment from some underlying or overlying source and emplaced upwards or downwards under abnormal pressure

(Berra and Felletti, 2011). The downward-tapering morphology is the evidence for loss of shear strength and fluidization velocity (Törö and Pratt, 2015). Downward emplacement of dikes has been attributed to Neptunian dikes related to the infilling of fissures (Montenat et al., 1991, 2007), reverse-density loading caused by earthquakes (Eyles and Clark, 1985), storm-wave activity (Martel and Gibling, 1993), dewatering due to compaction (Tanner, 1998), or earthquake activity (Pratt, 1998). Considering orientation, geometric relationships, and the nature of the infilling (Törö and Pratt, 2015), here the sedimentary dikes are interpreted as injection features induced by earthquakes. Sedimentary dikes cut by microfaults indicate a minor shock after the process of water escape when the layers are more lithified.

#### 3.1.2. Hydraulic shattering

**3.1.2.1. Description.** In well ST1H (see Fig. 2B for location) in Sequence III, a group of parallel veins of calcarenite are present in the massive calcilutite associated with many horizontal to slightly oblique minor veins or dikes. This structure is characterized by groups of arched calcarenite veins or dikes (Fig. 6A), with 4-cm-wide lenses of gravel-sized clasts between them. A single dike shows an enteroid or tabular shape surrounded by many linear minor dikes. The axial surface of this structure is exactly upright.

**3.1.2.2. Interpretation.** As the energy needed is fast growing, hydraulic shattering can occur where strong hydraulic forces cause calcarenite veins or dikes to spread laterally into the surrounding strata (Obermeier, 1996; Zhang et al., 2007; Ettensohn et al., 2011). The morphology of the dikes exhibits an obvious fluidization with liquefaction, including the addition of minor dikes. Clearly, there was a sudden upward-directed hydraulic force, believed to be the result of earthquake-induced liquefaction (Obermeier, 1996).

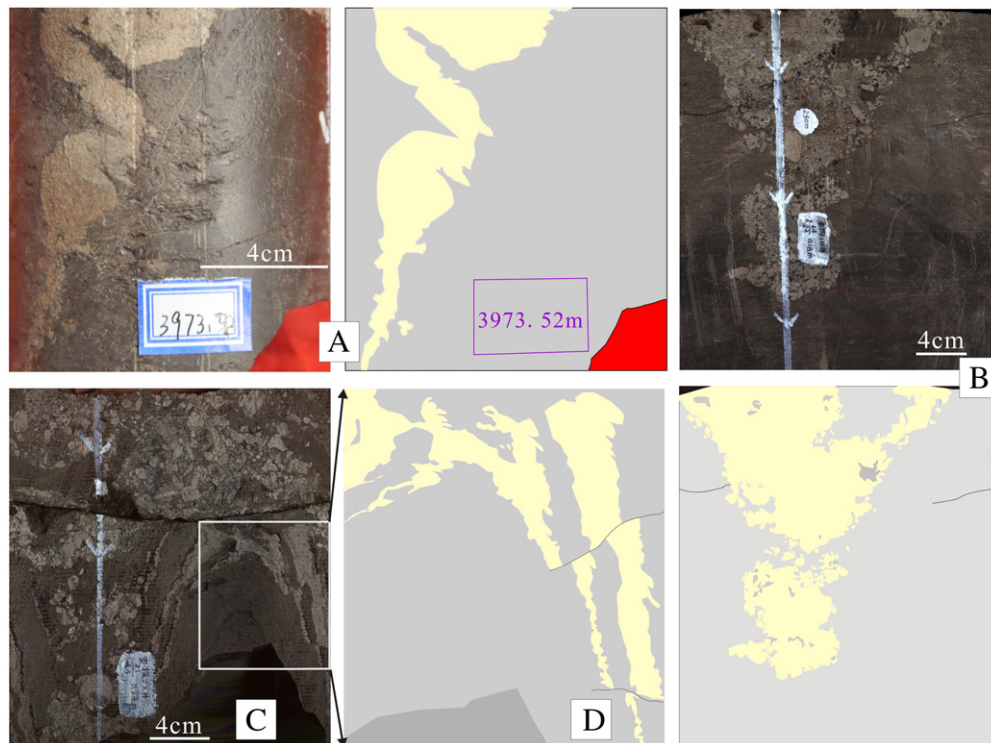


**Fig. 5.** Core image and tracing of sedimentary dikes in Sequence III from the lowermost submember of Es3 of the Shulu Sag of east China. For location of wells, see Fig. 2B. (A) Sausage-shaped calcarenite dike. From well ST1H, at 3973.52 m. (B) Breccia dike made up of subangular to subrounded gravel-sized carbonate clasts. From well ST1H, at 3961.6 m. (C) Calcareous dike associated with micro-faults. From well ST2X, at 3725.17 m. (D) Tracing of the calcarenous dike. Arrows indicate the direction of the bottom of the strata, not the top.

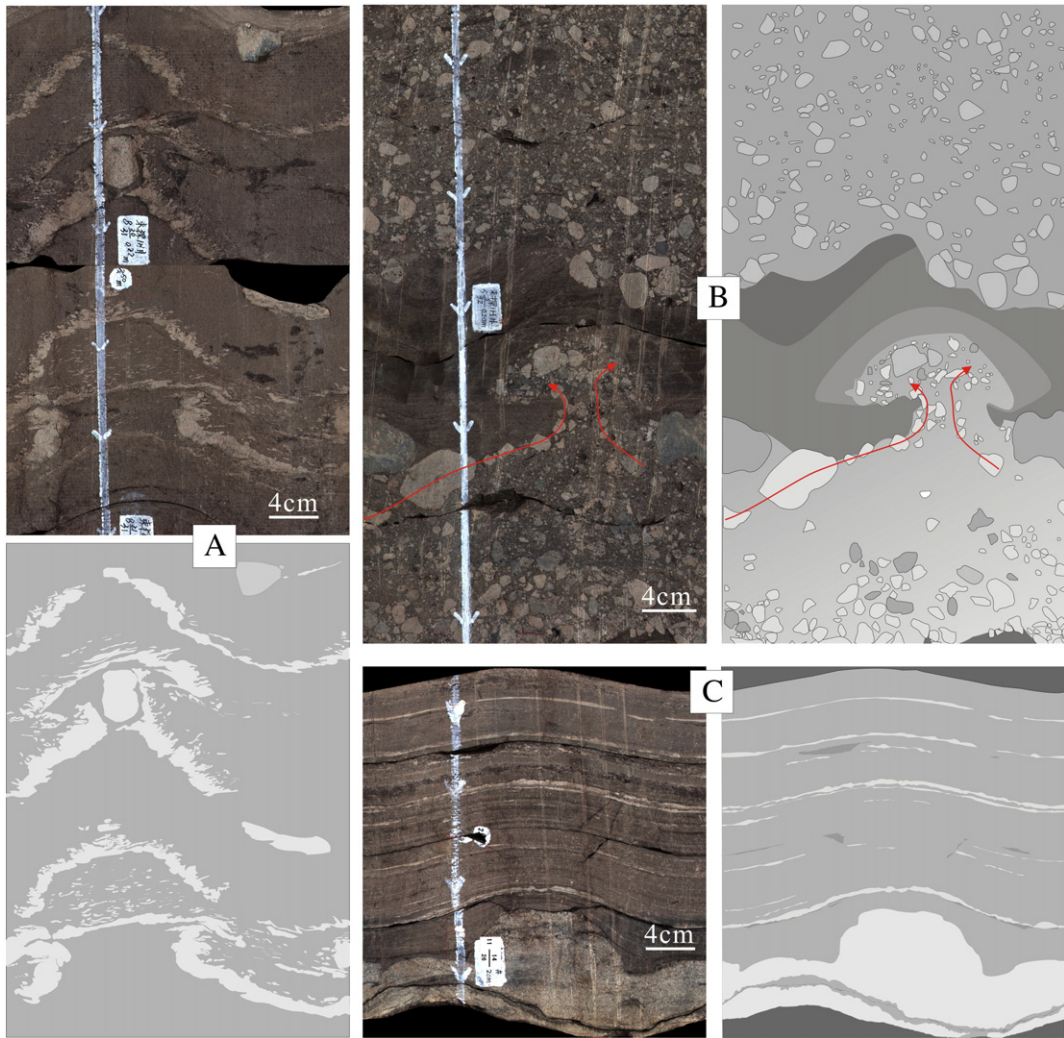


**Fig. 6.** Vertically scanned core image and tracing of ductile deformation structures in Sequence III in the lowermost submember of Es3 of the Shulu Sag from well ST1H (for location, see Fig. 2B). (A) Hydraulic shattering. A group of parallel-liquefied calcarenite dikes with many horizontal to slightly oblique minor dikes at 3993.1 m. (B) Mushroom-like diapir composed of carbonate gravels and silt-sized sediment at 3974.73 m. Note the long axis orientation of the gravels (red arrows). (C) Arched diapir. Water-saturated calcarenites intrude and deform overlying bed at 4080.1 m. Arrows indicate the direction of the bottom of the strata, not the top.

### 3.1.3. Diapir structures

**3.1.3.1. Description.** In the Shulu Sag, mushroom-like diapirs and arched diapirs are made of calcarenites or carbonate rudstones, which intrude and deform overlying laminates in Sequence III. The mushroom-like structures consist of gravel-sized clasts, of which the largest is 6 cm in length. The mushroom head shows a width of about 8 cm and a height of up to 4 cm (Fig. 6B). The outside lining of the mushroom cap is calcisiltite. Apart from the presence of the mushroom-like diapirs, domical diapirs have also been observed in the lowermost submember of Es3 of the Shulu Sag. These small domes contain coarse- to medium-grained calcarenite with dimensions of 10 cm in width and 5 cm in height (Fig. 6C). The overlying layer has been bent and fractures are generated right above the dome.

**3.1.3.2. Interpretation.** Many studies have described diapiric injection by silt-sized sediment or fine-grained sand (Chapman, 1983; Hempton and Dewey, 1983; Scott and Price, 1988; Mohindra and Bagati, 1996; Moretti, 2000; Rodríguez-Pascua et al., 2000, 2010; McLaughlin and Brett, 2004; Berra and Felletti, 2011). They are small diapir-like morphologies intruding upward, which are similar to “sand volcanoes” but

do not reach the surface (Montenat et al., 2007). The formation of the diapir-like structures may result from liquefaction and fluidization due to seismic shock or load-induced deformation (Berra and Felletti, 2011). Rapid loading of sediments is an interpretation discarded here based on the morphologic characteristics of these diapirs. The long axis orientation of the gravel-sized clasts in the mushroom-like structures demonstrates the upward flow of poor-sorted clasts as a quasi-fluid or viscous solid pushing into the overlying laminates. The bent overlying layer and the fractures above the dome indicate the forces of upward intrusion. Therefore, this structure can be confidently ascribed to a seismic activity rather than the load effects.

### 3.1.4. Convolute lamination

**3.1.4.1. Description.** Thickness of the disturbed laminae ranges from 1 to 20 cm. The morphology is irregular but laterally deformed synclines and anticlines with individual fold reaching up to 5–10 cm in height and averaging 5–10 cm in width (Fig. 7A) in Sequence III. These folded layers consist of interbeds of thin calcisiltite–calcilutite. The anticlinal flanks are gentle and there are no apparent sliding structures nor injection veins. The orientation of fold axes is almost upright (Fig. 7A) which is in contrast to randomly oriented axes in Fig. 7B. The orientation of

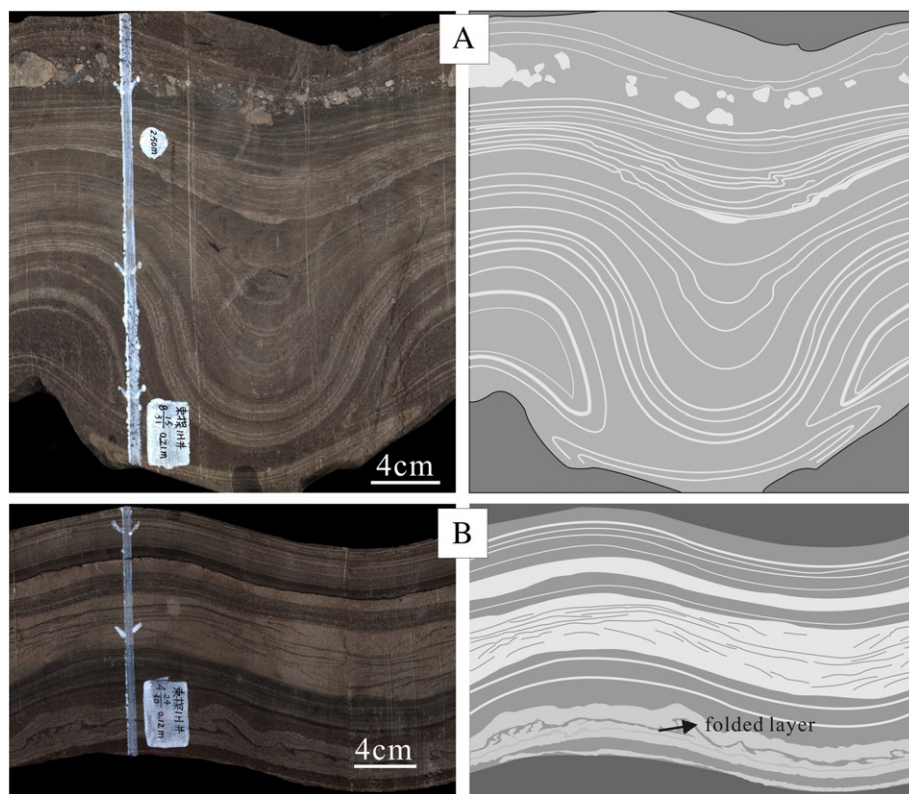


**Fig. 7.** Vertically scanned core image and tracing of convolute lamination in Sequence III from the lowermost submember of Es3. For location of wells, see Fig. 2B. (A) Deformation showing laterally alternating synclines and anticlines. From well ST1H, at 3992.07 m. (B) Folded layers with irregular fold axes without affecting underlying and overlying strata. From well ST1H, at 3972.55 m. Arrows indicate the direction of the bottom of the strata, not the top.

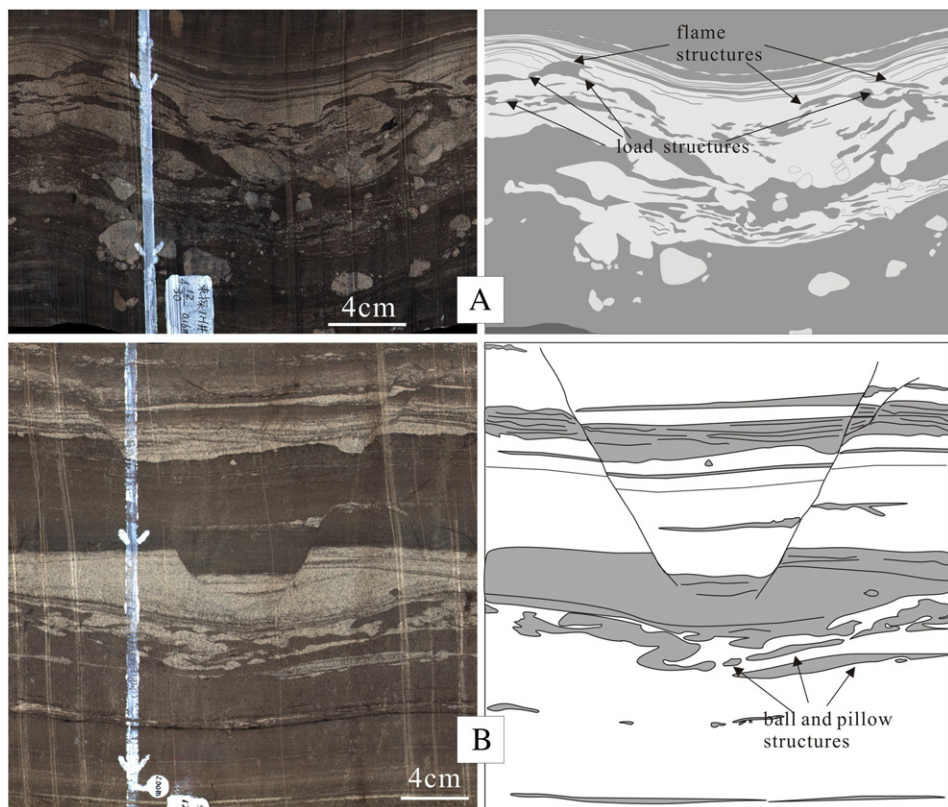


**Fig. 8.** Vertically scanned core image and tracing of load, flame, and ball-and-pillow structures in Sequence III from the lowermost submember of Es3. For location of wells, see Fig. 2B. (A) Load and flame structures. From well ST1H, at 3970.41 m. (B) Ball-and-pillow structure under a small synsedimentary fault. From well ST1H, at 4084.2 m. Arrows indicate the direction of the bottom of the strata, not the top.

fold axes varies from inclined to nearly horizontal and the fold amplitudes are about 2 cm (Fig. 7B). The bottom and top of a convolute laminated bed is separated by dark-gray calcilutite interbeds.

**3.1.4.2. Interpretation.** Convolute lamination is a kind of small-scale deformational structure within a calcarenite bed or thin calcisiltite–calcilutite layers where the overlying and underlying layers are undisturbed. It is formed when sediments are still unconsolidated. The origin of similar deformational structures has been attributed to loading pressures (Dzulynski and Smith, 1963), downslope slumping (Strachan, 2002; Alsop and Marco, 2011), and an elastic–plastic response of sediment to shear stress (Dzulynski and Smith, 1963; Hibsch et al., 1997; Rodríguez-Pascua et al., 2000; Rodríguez-López et al., 2007; Rana et al., 2013) by currents on the sediment surface, or an earthquake. On the basis of lithology similarity of convolute lamination and overlying beds and the fold morphology lacking uniform axial planes, sediment loading and slumping can be ruled out. Shearing by currents can be discarded due to lack of erosional disconformities between convolute lamination and superjacent deposits. Consequently, the structure is probably related to a hydroplastic deformation caused by earthquakes.

### 3.1.5. Load structures, flame structures, and ball-and-pillow structures

**3.1.5.1. Description.** These structures, found in Sequence III, show several centimeters wide asymmetric concave profiles of light-gray calcarenite over dark-gray undulating calcilutite (Fig. 8A and B). Scattered gravel-sized clasts of carbonate rock are mixed with medium- to coarse-grained calcarenite within the underlying laminae (Fig. 8A). The overlying beds are thin interbeds of calcisiltite and calcilutite that are undisturbed. Flame-like calcilutite protrudes upward into coarser calcarenite (Fig. 8A). A coarse sandstone bed with circular structures composed of calcarenite is detached from the overlying parent bed and forms similar

structures in the underlying calcilutite. Load and ball-and-pillow structures are present below a small synsedimentary fault in one example (Fig. 8B). Small-scale ball-and-pillow structures are nodules or elongated lenses made of fine-grained calcarenite about 0.1 cm in width (Fig. 8B).

**3.1.5.2. Interpretation.** These SSDSs show denser sediment sinking into less dense sediment (Suter et al., 2011) that behaves like a fluid or semi-fluid possibly during earthquake-induced liquefaction (Rana et al., 2013). They may form as a result of gravitational instabilities related to density differences or uneven loading (Lowe, 1975; Moretti et al., 1999; Neuerth et al., 2006; Moretti and Sabato, 2007). Alternatively, load structures may also form due to earthquakes (Du et al., 2008; Fortuin and Dabrio, 2008; Rana et al., 2013), as simulated by Owen (1996). Large-scale load structures (>0.5 m) can be interpreted as seismites (Moretti and Sabato, 2007), which nevertheless cannot be observed in the core. Flame structures appear always in association with load structures. And ball-and-pillow structures represent an advanced stage of load structures (Ghosh et al., 2012).

### 3.1.6. Loop bedding

**3.1.6.1. Description.** This structure, which is well developed in wells J97 and ST3 (see Fig. 2B for locations), occurs alone or in chains in Sequence III and Sequence V. It is made of interlaminated calcisiltite–calcilutite, giving morphologies of loops or links of concentric rings. In most cases the loop is 10 cm in width and the height ranges typically from 3 to 10 cm (Fig. 9A–C). This structure can be associated with laterally extensive folding and convolute lamination (see Fig. 9A). A lump of irregularly shaped calcarenite is present in the lower part of the biggest loop in Fig. 9B. Deformation in Fig. 9C can be described as a simple loop-like deformation at first glance. However, closer inspection shows that some or

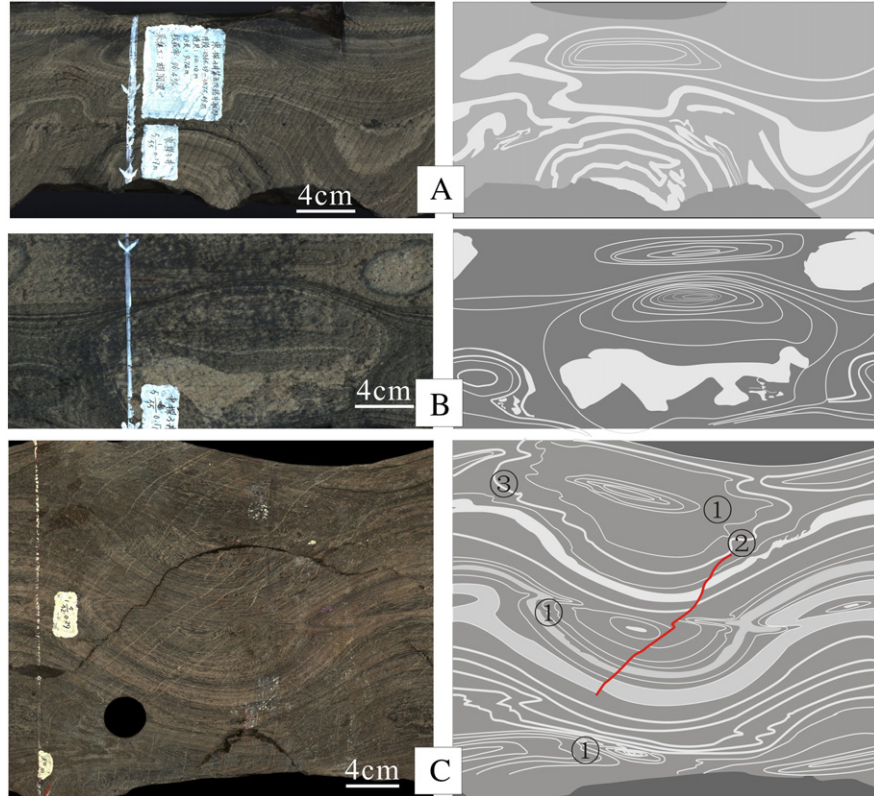


**Fig. 9.** Vertically scanned core image and tracing of loop bedding in Sequences III and V from the lowermost submember of Es3. For location of wells, see Fig. 2B. (A) Concentric loops with convolute lamination. From well ST3, at 3865.56 m. (B) Loop bedding. Note the complex deformation of calcarenite. From well ST3, at 3866.29 m. (C) ① Loop bedding, ② microfault, and ③ convolute lamination. From well J97, at 3449.24 m. Arrows indicate the direction of the bottom of the strata, not the top.

all of the individual layers are convolute laminae interpenetratively deformed and there is a microfault filled with calcite across two sets of "loops."

**3.1.6.2. Interpretation.** These SSDSs are interpreted as loop beddings consisting of multiple-ringed concentric lamellae that are connected laterally. They are different from the chain-like loop beddings described by Calvo et al. (1998) and Rodríguez-Pascua et al. (2000) in appearance. The loop beddings here have convolute laminae and normal micro-faulting displaying a ductile–brittle behavior of unlithified to progressively more lithified laminated sediments (Fig. 9C). This structure is interpreted as a result of tensile stress of successive minor seismic shocks (Calvo et al., 1998; Rodríguez-Pascua et al., 2000; Yuan et al., 2006). The development of loop bedding is thought to reflect the low magnitude of earthquakes.

### 3.1.7. Subsidence structure

**3.1.7.1. Description.** The laminae of calcilutite are bent downward with minor disruption by large gravel-sized clasts of weathered carbonate rock (Fig. 10A and B) in this structure found in Sequence III and V. Size of these clasts varies from 0.5 to 5 cm and the direction of long axes varies from upright to inclined to recumbent. The laminae exactly under the gravel-sized clasts have been significantly distorted.

**3.1.7.2. Interpretation.** Bent laminae appear to result from an interstitial overpressure and a drastic decrease in shear strength within the calcilutite. The most important driving force might be an unstable density gradient. This overloading process is related to liquefaction induced by the rapid input of sediment on a soft substratum (Moretti et al., 2001). Deformation occurred when the underlying laminated calcilutite was poorly consolidated and water-saturated. It is assumed that weathered rock from the nearby Ningjin uplift fell into soft sediment from a great height to form the dispersed gravel-sized clasts. The trigger mechanism may be earthquake activity.

### 3.1.8. Other structures

**3.1.8.1. Description.** One-centimeter-wide symmetric but elliptical shape composed of fine-grained calcarenite occurs in the calcilutite below the overlying strata of calcarenite in Sequence III (Fig. 11A and B). On its right, long or thick pores are present in an approximately horizontal

direction and they are filled with sediments from an overlying layer. Many small-scale nodules or balls consisting of fine-grained calcilutite and calcarenite (Fig. 11C and D) occur in the massive calcilutite under calcarenite beds. Most of them are about 0.1 cm in width and generally show irregular shapes.

**3.1.8.2. Interpretation.** Morphology of these deformation structures is similar to load structures induced by liquefaction. The structures in Fig. 11A and B can be interpreted as calcarenite-filled burrows. The millimeter-thick nodules or balls (Fig. 11C and D) can be attributed to bioturbation by animals moving through the layers of alternating lithology (Moretti and Sabato, 2007).

## 3.2. Synsedimentary faults

### 3.2.1. Description

Various types of synsedimentary faults clearly moved consolidated to less consolidated strata vertically or at an angle are present in Sequence III and Sequence V of many wells, including small graben structures in wells ST3, ST1H, and J85 (Fig. 12A–C), microfaults in well ST1H (Fig. 12D and E), and a series of microfaults in well J97 (Fig. 12F) (see Fig. 2B for the location of these wells). Some of the fault planes that are filled with sediments are flat (Fig. 12C), and some are irregular (Fig. 12B, D, and E). A great majority of synsedimentary faults are normal faults between the unaffected upper and lower layers. The lithologies of the disturbed sediment generally consist of fine- to medium-grained calcarenite and locally calcilutite; however, there are exceptions, including pebble-sized carbonate gravel appearing in a synsedimentary fault (Fig. 12B). The dip angle of the faults is large, about 50 to 80° with offsets varying between 0.2 and 2 cm. In addition, the thickness across the fault is incongruent in Fig. 12B, D and E.

### 3.2.2. Interpretation

Some synsedimentary fault planes were not planar originally because the sediments were not well consolidated and responded with a ductile behavior (Mohindra and Bagati, 1996; Rossetti and Góes, 2000; Neuwerth et al., 2006). Straight fault surfaces indicate brittle failure of relatively consolidated material. Most of synsedimentary faults are interpreted as a result of seismic activities (Pratt, 1994; Mohindra and Bagati, 1996; Bhattacharya and Bandyopadhyay 1998; Kahle, 2002; Fortuin and Dabrio, 2008; Taşgin et al., 2011; El Taki and Pratt, 2012; Törö and Pratt, 2015). Differential compaction may cause small-scale

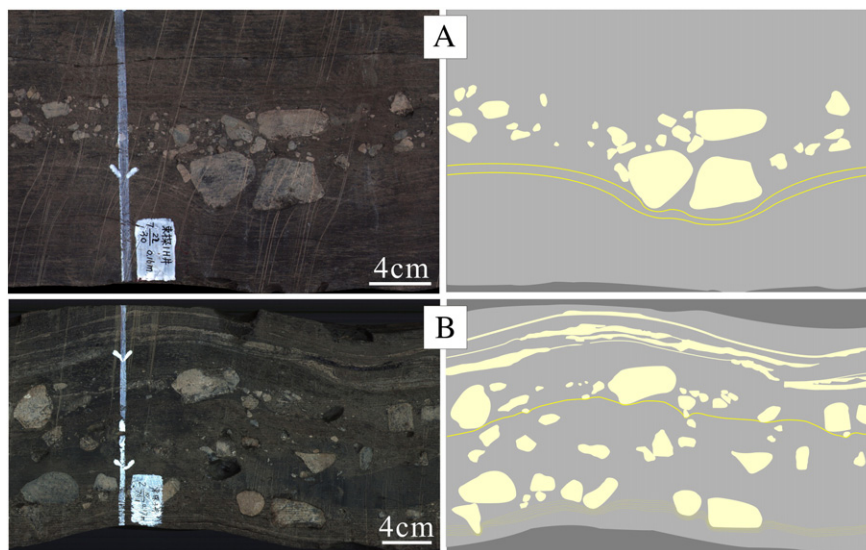


**Fig. 10.** Vertically scanned core image and tracing of subsidence structures in Sequences III and V from the lowermost submember of Es3 of the Shulu Sag. For location of wells, see Fig. 2B. (A) Bent laminae of calcilutite from well ST1H, at 3988.05 m. (B) Deformed bedding from well ST3, at 3676.84 m. Arrows indicate the direction of the bottom of the strata, not the top.

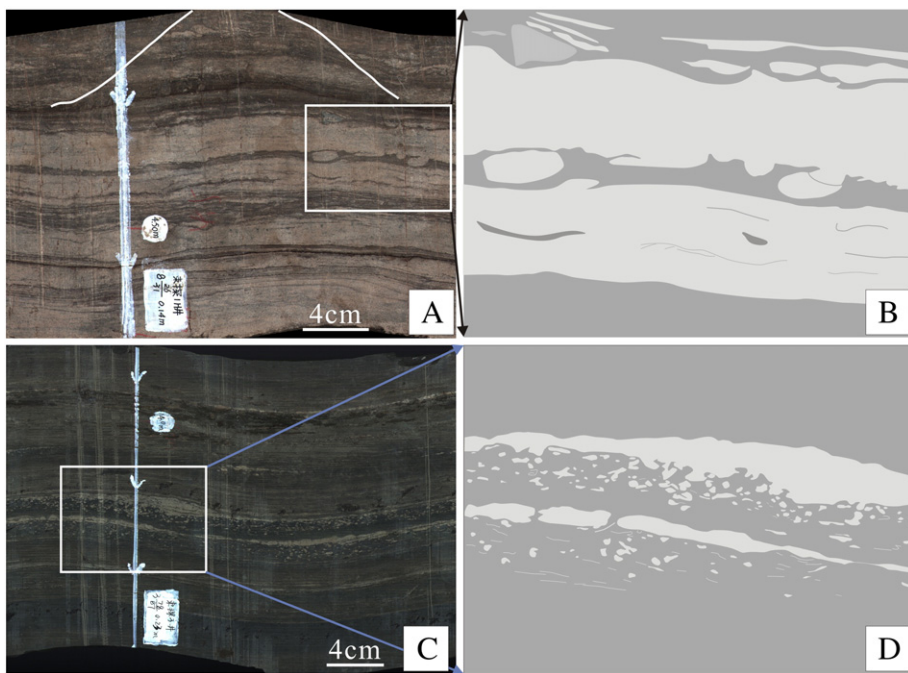


**Fig. 11.** Other structures in Sequences III from the lowermost submember of Es3 of the Shulu Sag. For location of wells, see Fig. 2B. (A)–(B) Bioturbation traces. From well ST1H, at 3993.97 m. (C)–(D) Small-scale nodules or balls. From well ST3, at 3802.78 m. Arrows indicate the direction of the bottom of the strata, not the top.

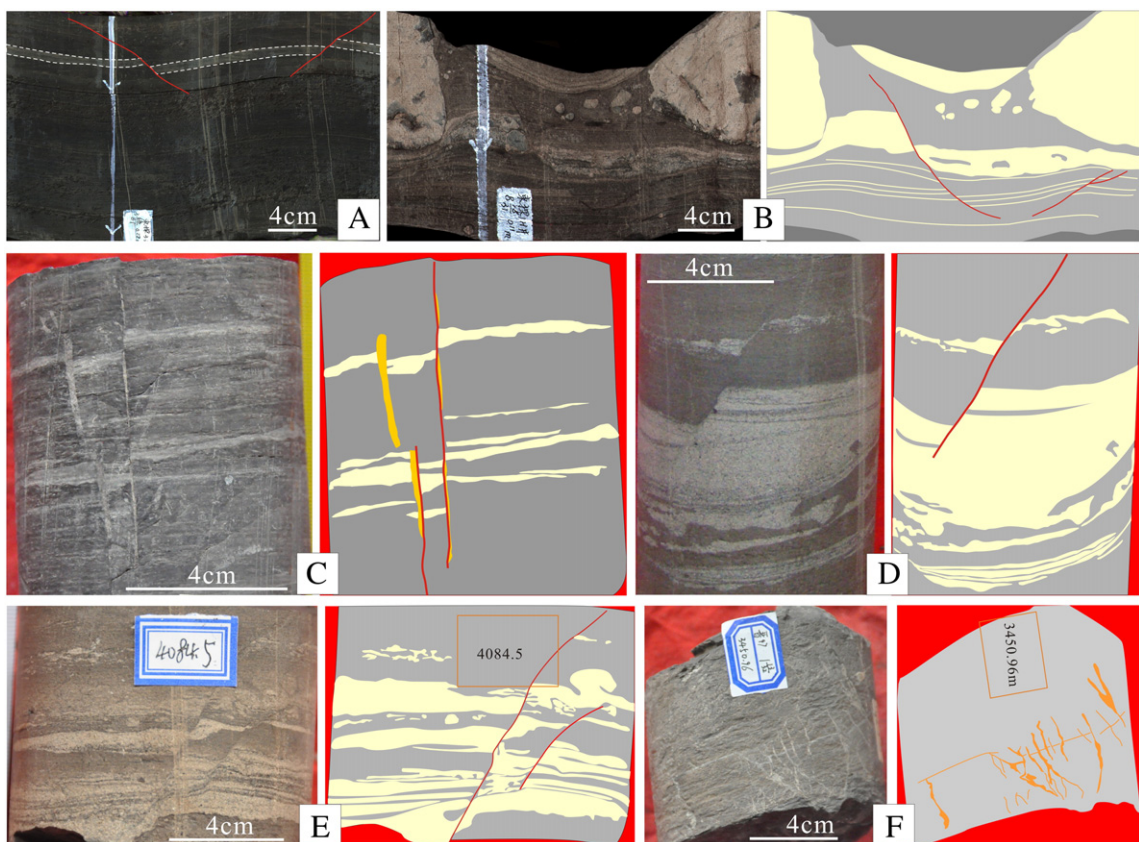


**Fig. 12.** Various types of synsedimentary faults in Sequences III and V from the lowermost submember of Es3 of the Shulu Sag. Well locations are found in Fig. 2B. (A) Small-scale graben. From well ST3, at 3800.94 m. (B) Pebble-sized clasts appear in a synsedimentary fault. The faults disappear downwards and do not affect the underlying laminated deposits. From well ST1H, at 3992.18 m. (C) Small-scale graben. From well J85, at 3770.95 m. (D) Normal faults. From well ST1H, at 4084.43 m. (E) Normal faults. From well ST1H, at 4084.5 m. (F) A series of microfaults. From well J97, at 3450.96 m. Arrows indicate the direction of the bottom of the strata, not the top.

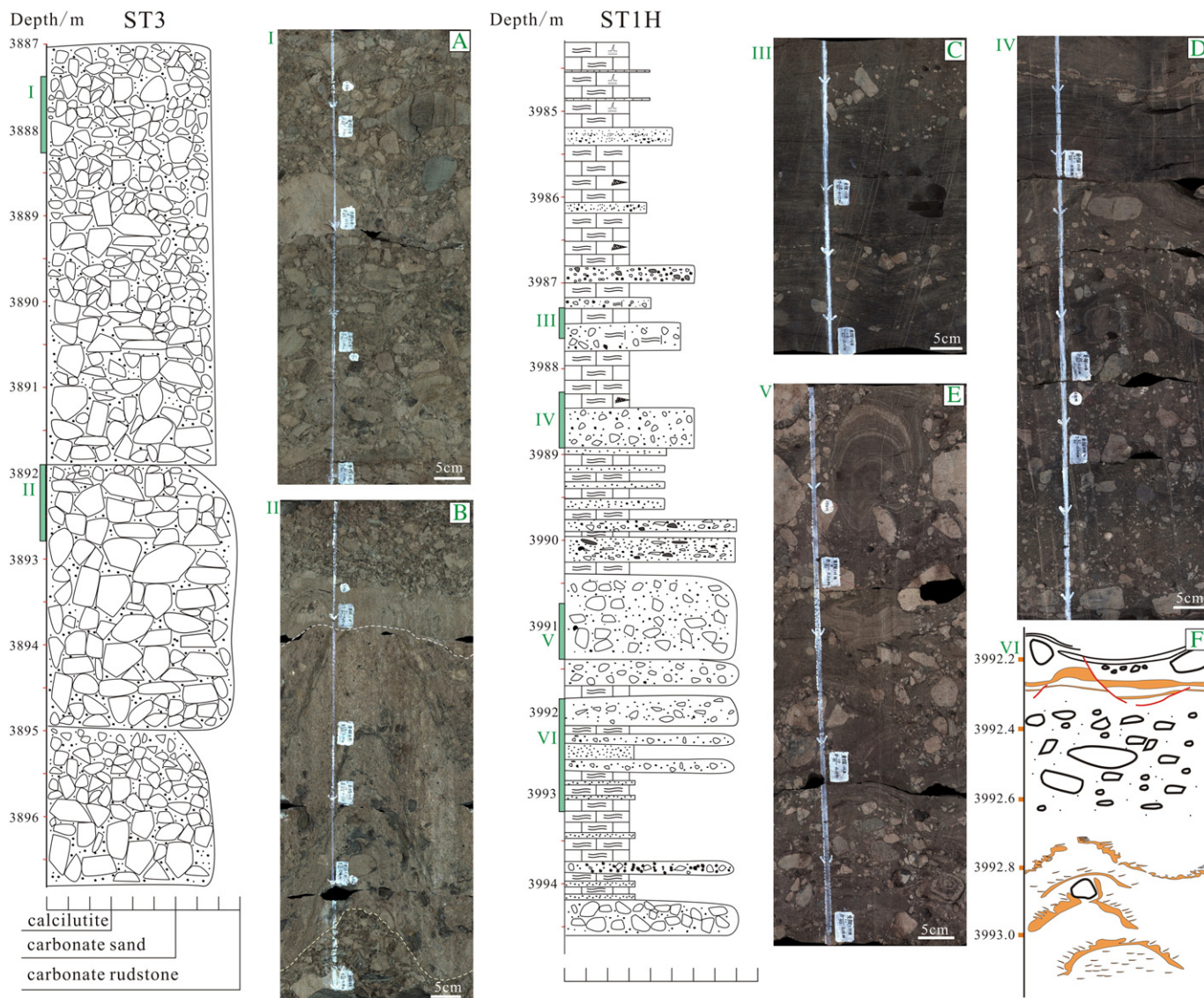


**Fig. 13.** Seismoturbidites of Sequence III in the lowermost submember of Es3 in wells ST3 and ST1H of the Shulu Sag. The clast-supported rudstone in well ST3 consists of angular-subangular coarse clasts poorly sorted, with random directions for the major axes of the clasts. Abundant soft-sediment deformation structures are in the matrix-supported rudstone of well ST1H, such as calcarenous dikes and hydraulic shattering. Arrows indicate the direction of the bottom of the strata, not the top.

faults as well (Fortuin and Dabrio, 2008; Törö and Pratt, 2015), whereas such a mechanism is not possible here as the overlying bed is mainly laminated calcilutite or massive calcilutite, same as the faulted bed. A seismic origin is more probable.

### 3.3. Slumps

#### 3.3.1. Seismoturbidites

**3.3.1.1. Description.** A large rudstone bed of Paleozoic carbonate clasts from the Ningjin uplift with poor sorting appears in well ST3 over a total thickness of 100 m (see Fig. 2B for location) within Sequence III. The rudstone is generally clast-supported with normal grading or structureless. The gravel-sized clasts (few millimeters to 1 m in length) range from angular, subangular, to subrounded with a matrix composed of calcilutite. The direction of major axes of the clasts is random, recumbent, inclined, or upright (Fig. 13A, B). Lithology of the clasts includes crystalline dolomite, micrite, oolitic limestone, bioclast limestone, and flat-pebble rudstone.

By contrast, in well ST1H (location in Fig. 2B) there is matrix-supported rudstone containing significant soft-sediment deformation.

The clasts are 0.5–10 cm in diameter, subangular to subrounded. The matrix is calcilutite, calcarenous, and pebbly rudstone, mixed with organic matter and pyrite. Poorly sorted gravel-sized carbonate clasts in Fig. 13C constitute a loop that is roughly 10 cm wide and 8 cm high. Vortex-like structures composed of calcisiltite–calcilutite or calcarenous are distributed in the matrix of the rudstones in Fig. 13D and E. Matrix-supported rudstone with subangular clasts floating in the dark-gray matrix is intermingled with soft-sediment deformation, such as recumbent sedimentary dikes (Fig. 13D) and hydraulic shattering (Fig. 13F). Furthermore, syndepositional faults with 2 cm offsets were discovered in the matrix-supported rudstone of well ST1H (Figs. 12B, 13F) at 3992.18 m.

**3.3.1.2. Interpretation.** Gravity flow deposits triggered by an earthquake and those triggered by changes in climate or sedimentation rates are difficult to distinguish (Gorsline et al., 2000; Shiki et al., 2000; Bertrand et al., 2008; Carrillo et al., 2008; Fanetti et al., 2008; Wagner et al., 2008; Van Daele et al., 2014) since they all contain massive bedding and graded beds (Nakajima and Kanai, 2000). Lithology, geochemistry, chronology, and physical properties can be used in the assessment of paleoearthquake activity (Gorsline et al., 2000; Wagner et al., 2008;

Leroy et al., 2010; Faridfathi and Ergin, 2012) in finer-grained sediments, but difficult in sediments composed of gravel-sized clasts. Seismoturbidites are the products of gravity-flow deposits as a response to seismic activity (Mutti et al., 1984), including debris-flow deposits and turbidites. Megaturbidites have been generally regarded as the result of an earthquake (Mutti et al., 1984; Séguert et al., 1984). The thickness of the clast-supported rudstone in Sequence III of well ST3 (Fig. 13A and B) is up to 100 m. They can be considered as megaturbidites. There is no steep-slope paleotopography in the ST1H well area to form gravity-flow deposits along the slope of the Shulu Sag, as noted in the geometries of these beds (Fig. 3). Such continuous and thick rudstone could not be the result of wave action or flood deposition, because the large clasts are poorly sorted and most of them are angular. In addition, there is no sedimentologic evidence for storm activity within these successions. Due to the lack of other feasible mechanisms, these rudstones are interpreted as slumps caused by earthquakes.

Turbidites were probably triggered by an earthquake if the sediments have a close relationship with autochthonous seismites. Syndepositional faults, which were discovered in the turbidites of well ST1H (see Figs. 12B, 13F) at 3992.18 m of Sequence III, suggest synchronicity of the seismites and turbidites. Also, many SSDSs are present with matrix-supported rudstone in this Sequence of well ST1H (Fig. 13D–F). All of these provide strong evidence for an interpretation that the trigger mechanism of these debris-flow deposits or turbidites was indeed the earthquake activities.

### 3.3.2. Mixed-source rudstone

**3.3.2.1. Description.** Mixed-source rudstone is relatively common in Sequence III of the Shulu Sag. This lithofacies contains two kinds of

clasts. One is Ordovician and Cambrian carbonate rocks transported from the Ningjin uplift, and the other is Paleogene intrabasinal gravel-sized micritic intraclasts. The color of Paleozoic carbonate clasts is light gray or gray, and the size is smaller than the Paleogene intraclasts (Fig. 14A). The Paleogene clasts are mainly angular to subangular micritic limestone and dolomite clasts with poor sorting from Ningjin uplift. The Paleogene intraclasts also have obvious boundaries, but are deformed. These intraclasts show deformational characteristics of soft sediment such as elongation or squashed textures (Fig. 14B and C), giving lacerated or subrounded morphology (Fig. 14A–C). The composition of the Paleogene intraclasts is dark-gray, massive calcilutite with shelly fossils, small quartz grains, pyrite, and organic matter. Transport clearly occurred while the rock clasts were unconsolidated. Twenty centimeters length of calcarenite dikes and microfaults with 0.5 cm offsets are present in the mixed-source rudstone in Sequence III of well ST2X (Fig. 5C and D).

**3.3.2.2. Interpretation.** Mixed-source rudstone is interpreted to be a special manifestation of debris-flow deposits generated by earthquake activity. Gravel-sized micritic intraclasts transported while unconsolidated are similar to rip-up intraclasts of the eastern Alboran Basin (Braga and Comas, 1999). They may be derived from erosion by the gravity flow on the underlying calcilutite substratum. Calcareous dikes and microfaults are usually considered to be induced by seismic movements (Pratt, 1998; Fortuin and Dabrio, 2008; Taşgin et al., 2011; Törö and Pratt, 2015), and their presence in association with the rudstone demonstrates a direct link between the mixed-source rudstone and seismicity.

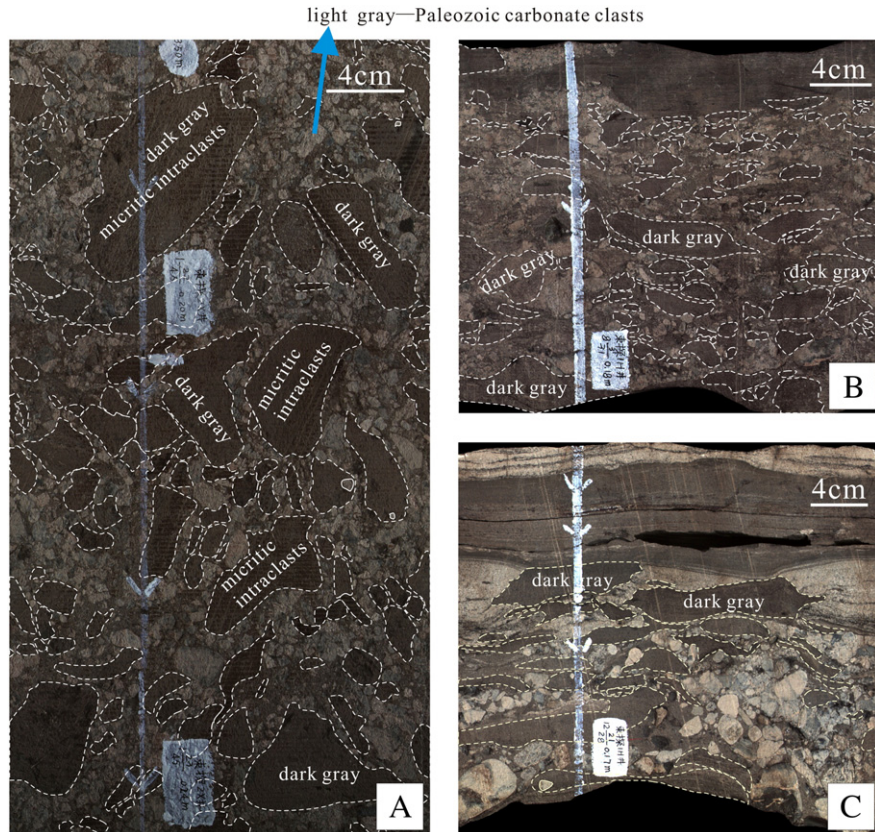


**Fig. 14.** Mixed-source rudstone in Sequence III from the lowermost submember of Es3 of the Shulu Sag. The dark-gray parts are Paleogene micritic intraclasts mixed in with the Paleozoic light-gray carbonate clasts. The matrix is calcilutite. The micritic intraclasts are elongated or squashed as well as lacerated or subrounded. See Fig. 2B for well locations. (A) From well ST2X, at 3725.2–3725.61 m. (B) From well ST1H, at 3989.89 m. (C) From well ST1H, at 4086.34 m. Arrows indicate the direction of the bottom of the strata, not the top.

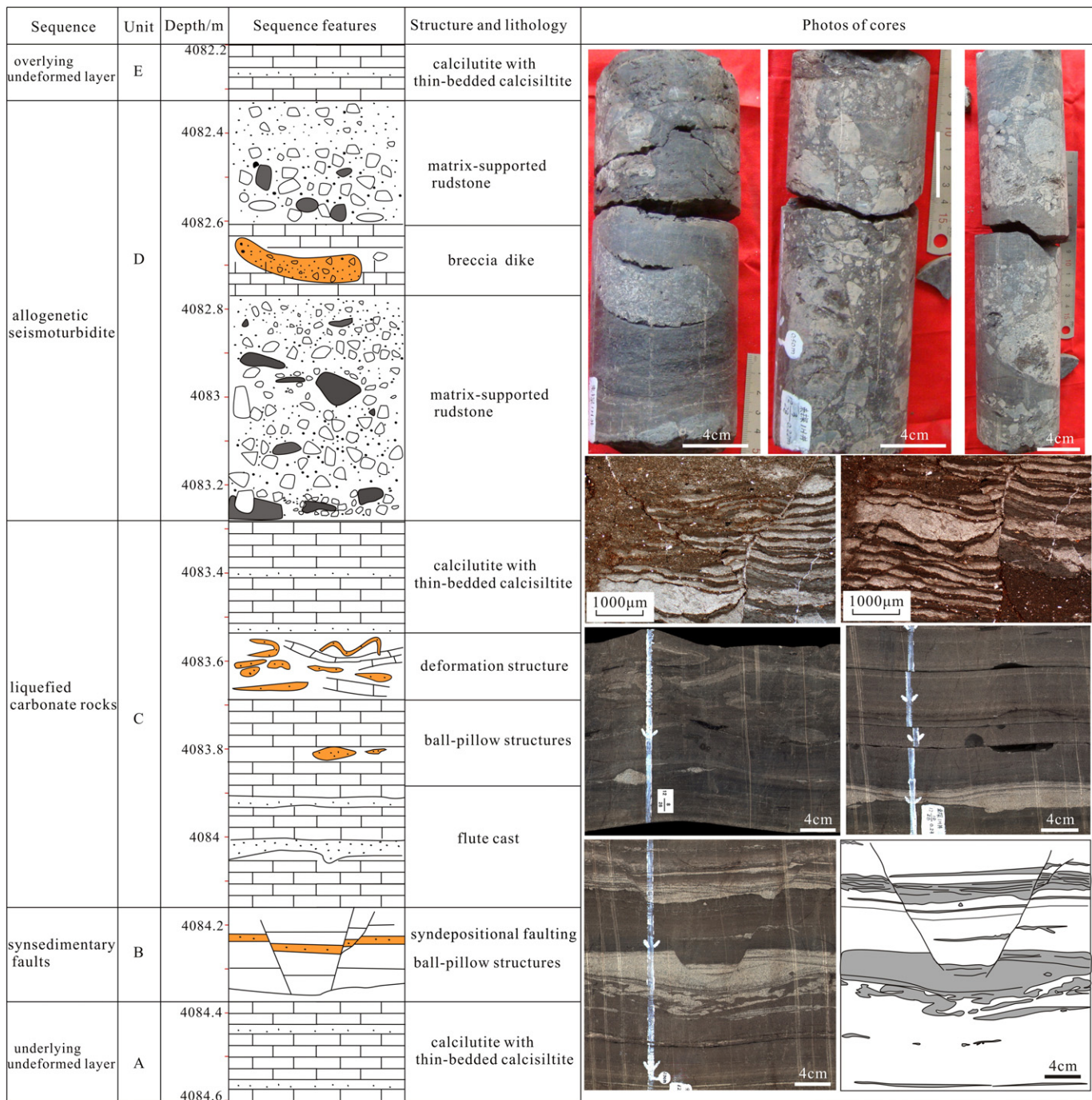


**Fig. 15.** Seismites sequence in well ST1H from Sequence III in the lowermost submember of Es3 of the Shulu Sag. From the base to the top: underlying undeformed layer, synsedimentary faults, liquefied carbonate rocks, allogenic seismoturbidite, and overlying undeformed layer. The pattern of deformation in this sequence reflects the changing energy levels during an earthquake. Arrows indicate the direction of the bottom of the strata, not the top.

### 3.4. Seismites sequence

The most sensitive sediments to the earthquake activity are fine-grained materials (Moretti et al., 1999; Owen and Moretti, 2011). For this reason, seismites develop more readily in deltaic plains and lacustrine environments, where such silty deposits, including a large volume of water for saturation of sediments, are common.

A complete vertical sequence of about 2.4 m thick found through core observation in well ST1H in Sequence III (see Fig. 2B for location) shows, from the base to the top: (A) underlying undeformed layers, (B) synsedimentary faults, (C) liquefied carbonate rocks, (D)

seismoturbidites, and (E) overlying undeformed layers (Fig. 15). Before an earthquake, the consolidation strata were undisturbed, that are, the underlying undeformed layers (A), composed of calcilutite with thin-bedded calcisiltite. When a quake was initiated, the consolidation strata were unaffected while ductile strata tended to flow or brittle deformation occurred under stress for existing unconsolidated and semisolid sediment. Next, a layer containing syndepositional faults (B) formed a small graben associated mainly with some small load and ball-and-pillow structures. As the seismic activity reached a climax, liquefaction started. The main lithology of unit C (liquefied carbonate rocks) was calcilutite and minor calcisiltite and the structures comprised flute

casts, ball-and-pillow structures, and some deformation. In the upper part of this unit, microfaults were observed through the microscope. Then, energy started to decay and alloogenetic seismoturbidites (D) which are from Ningjin uplift and composed of “matrix-supported rudstone” with Paleozoic clasts of varying sizes, were deposited. Breccia dikes were present in this layer as well. After the earthquake, undeformed sediments continued to be deposited, showing an abrupt contact with the underlying turbidite segment. The overlying undeformed layer (E) was calcilutite with thin-bedded calcisiltite, about 2 m thick (part of it is shown in Fig. 15). This seismites sequence reflects the seismic process of increasing then decreasing energy levels.

Sedimentary sequence patterns reflect the depositional process of an earthquake. The composition of a seismites sequence may be not exactly the same in all cases (Mutti et al., 1984; Song, 1988; Qiao et al., 1994). Sequences of seismic events were first described as (from the base) consisting of undisturbed beds, fault-grading beds, a rubble zone, a homogenized zone, and undisturbed beds (Seilacher, 1969; 1984). A complete sequence of a calcareous megaturbidite induced by earthquakes can be up to 5–30 m (Mutti et al., 1984; Séguert, et al., 1984), which has similar components and reflects the same change in energy. A seismite–tsunamite sequence with hummocky bedding represents an earthquake event with a related tsunami event (Song, 1988; Qiao et al., 1994; Du et al., 2001). Sequence A–B–C–D–E reflects the whole process of a strong seismic event from initiation to culmination, then decline and cessation (Fig. 15). Like in any other sedimentary sequence (e.g., Bouma sequences), some unit or units may be absent in the section (Qiao et al., 1994). Incomplete combinations, such as C–D–E and D–E, are very common. The full pattern of a seismites sequence is controlled by the magnitude of the earthquake, lithology, and the structural position where an earthquake occurred (Yuan, 2004).

## 4. Discussion

### 4.1. Origin of deformation

Morphologic characteristics of deformed structures are controlled by the initial rheologic properties of the sediment and the driving-force system, not by the trigger (Owen, 1987; Ezquerro et al., 2015). Consequently, it is difficult to distinguish between seismically and non-seismically induced SSDSs (Owen and Moretti, 2011). However, analysis of morphology and the sedimentary and tectonic context will aid in determining the mechanism promoting sediment deformation (Törö et al., 2015; Törö and Pratt, 2015).

Several SSDSs can be attributed to endogenic processes, such as bioturbation (Fig. 11A–D). Lack of evidence for subaerial exposure precludes a desiccation origin. No ripple cross-lamination or hummocky cross-stratification indicating storm deposits (Molina et al., 1998; Alfaro et al., 2002) is present in the lowermost submember of the Shahejie 3 of the Shulu Sag.

In view of the tectonic setting, the best explanation for the trigger mechanism for these SSDSs is syndepositional to post-depositional earthquakes. The following factors point to a seismic triggering agent within the sediments of the lacustrine Shahejie Formation: (i) seismites are widely distributed in the Shulu Sag, such as in wells ST1H, ST3, J85, J97, and J116X (see Fig. 2B for locations). (ii) There are multiple sets of stacked “seismites” separated by undeformed beds. (iii) Seismites of Paleogene age have also been found in the nearby Paleocene Jinxian Sag (location shown in Fig. 2A) of the Jizhong Depression that is similar in structure to the Shulu Sag (Yang et al., 2014). Those interpreted seismically induced structures include water-escape channels, load casts, flame structures, ball-and-pillow structures, and micro-synsedimentary faults. (iv) Structural association of synsedimentary faults with sedimentary dikes, load structures, and loop bedding has been interpreted as concurrently seismically deformed (e.g., Kahle, 2002; El Taki and Pratt, 2012; Wallace and Eyles, 2015). (v) Similar SSDSs have been reproduced in the laboratory through the modeling

of earthquake effects in water-saturated soft sediments (Owen, 1996; Moretti et al., 1999). (vi) Growth indices of the nearby NW-trending Taijiazhuang fault and the NNE-trending Xinhe fault during the third member of the Shahejie Formation (Kong et al., 2005) indicate that these faults could have controlled the topographic relief within the basin and exerted a great influence on the distribution of sediment and its deformation.

### 4.2. Episodic activities

Similar to modern earthquakes, paleoearthquakes may be episodic (Qiao and Li, 2009; Qiao et al., 2013). A seismic active period normally has a number of activity events in succession. An ancient earthquake record comprises some deformation of sediment layers (Qiao et al., 2013). Several seismite layers separated by undeformed sediments can be considered as an earthquake episode. A number of episodes compose an active period when the time interval between two episodes is longer than the time between its separate earthquake sedimentary records. The long time interval is manifested by a thick succession of undeformed sediments between two episodes in stratigraphic sections. In the observation of outcrop or core, if there are multiple soft-sediment deformation and brittle deformation layers in a succession, it is most probable that the deformation was caused by ancient earthquakes, not by other factors (Qiao et al., 2013).

In the core from well ST1H located in the hanging wall of the Xinhe fault (see location in Fig. 2B), about 20 activity events (in blue) are recorded based on soft-sediment deformation patterns. They can be interpreted as nine seismic episodes and two active phases. One is colored pink from 3959 to 3994.4 m and the other is light green from 4072 to 4087 m (Fig. 16). More than 10 layers of soft-sediment deformation within a 10-m length of core are present (e.g., 3985–3994.4 m and 4077.6–4087 m). Soft-sediment deformation recurring intensively within strata over several meters may be explained best as seismic origin.

### 4.3. Relationship of seismites, seismicity, and sequences

Seismites can provide information about the magnitude and occurrence of ancient earthquakes. Soft-sediment deformation is mainly distributed in Sequence III from the lowermost submember of Es3 in the Shulu Sag (Fig. 17). Allochthonous seismoturbidites and mixed-source rudstone are well developed here. In comparison, fewer seismites exist in other sequences, but this may be due to the distribution of the drilled cores. However, considering the impact of the earthquakes on underlying consolidated strata, the fractures in Sequence III are more rare than in Sequence I and Sequence II, which points to earthquake activity in Sequence III that is perhaps more substantial than that in Sequence IV and Sequence V. Earthquakes may have occurred during the deposition of Sequence IV and Sequence V, but much weaker in intensity.

Loop bedding and subsidence structures are the main types of seismites in Sequence V (Fig. 17). The core located in Sequence IV of well J97 is <5 m thick, composed of calcisiltite, and is undisturbed, so minimal seismic activity in IV is inferred. In Sequence II, there are almost no soft-sediment liquefied and compressional structures and just one or two small-scale faults. In Sequence I, no seismites are present. Earthquakes appear to have been most active in Sequence III during the deposition of the lowermost submember of Es3 in the Shahejie Formation of the Shulu Sag, east China (Fig. 18).

### 4.4. Petroleum geologic significance

Void space of the Shulu reservoir includes intragranular pores, intergranular pores, fissures, and micropores. Intragranular pores can be further divided into two types: intercrystalline pores that originated in carbonate rocks and intragranular pores produced from the dissolution

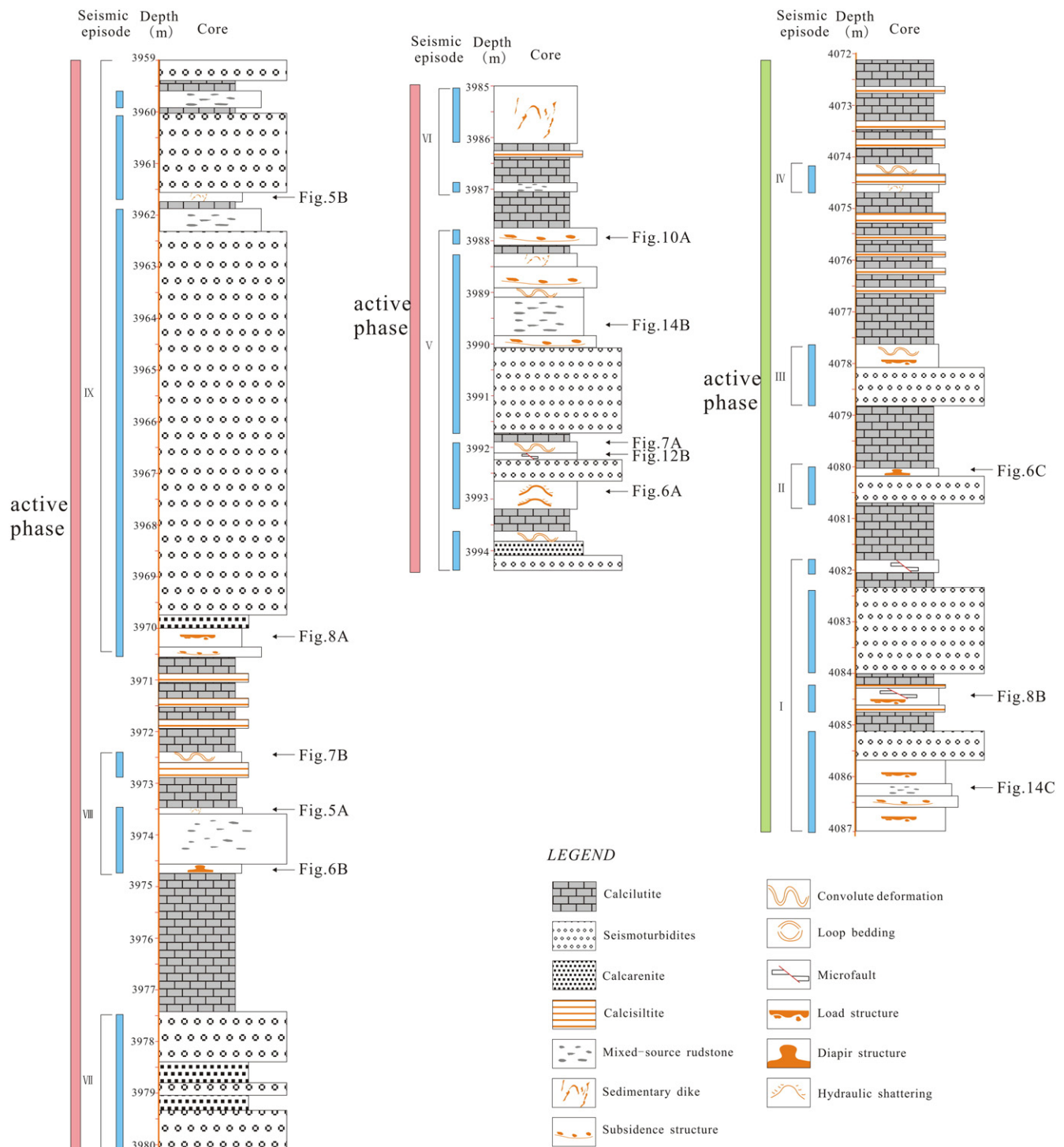


**Fig. 16.** Soft sediment deformation in well ST1H (see Fig. 2B for location) in Sequence III from the lowermost submember of Es3 of Shulu Sag. An ancient earthquake record comprises SSDSs, seismoturbidites, or mixed-source rudstones. Each section can be considered as an activity event (in blue). They are separated by thin undeformed layer. Several seismite layers separated by thick undeformed sediments can be considered as an earthquake episode. A number of episodes compose an active period. About 20 activity events (blue) are present, which can be interpreted as nine seismic episodes and two active phases. One is colored pink from 3959 to 3994.4 m and the other is light green from 4072 to 4087 m.

of chert or other clasts. Intergranular pores are pores that are preserved between clasts, including primary intergranular pores and secondary intergranular pores from dissolved matrix or cement (Liu et al., 2012). It is extremely subjective, imprecise (Giles, 1987; dos Anjos et al., 2000) and difficult to distinguish intergranular secondary pores generated through cement dissolution from primary intergranular pores. Fissures include structural fissures cutting through gravels and diagenetic

shrinkage fractures in a random manner. Micropores are mainly present in the massive calculitite, laminated calculitite, or the matrix of rudstones as dissolution features or primary pores.

#### 4.4.1. Ductile deformation

Thick, tight calculitite intervals tend to serve as permeability barriers (Song et al., 2004). Sedimentary dikes can cut through these barriers

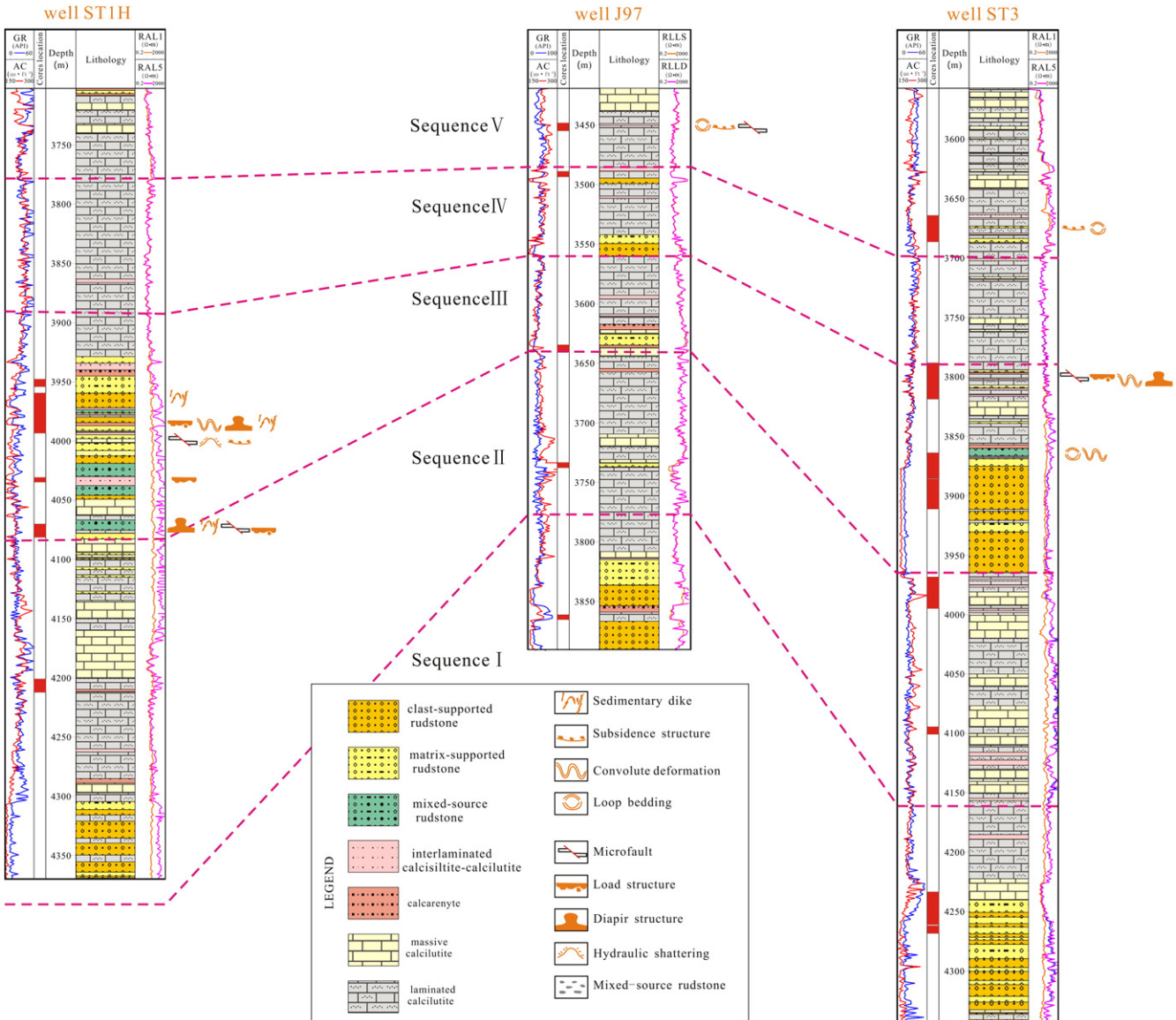


**Fig. 17.** Distribution of seismites in the cores from the lowermost submember of Es3 of the Shulu Sag. See Fig. 2B for locations. Soft-sediment deformation is mainly present in Sequence III and fewer seismites exist in other sequences. It can be inferred then that the earthquakes are most active in Sequence III and weaker to absent in the other sequences. The red pillars in the second column show the location of the drilling core.

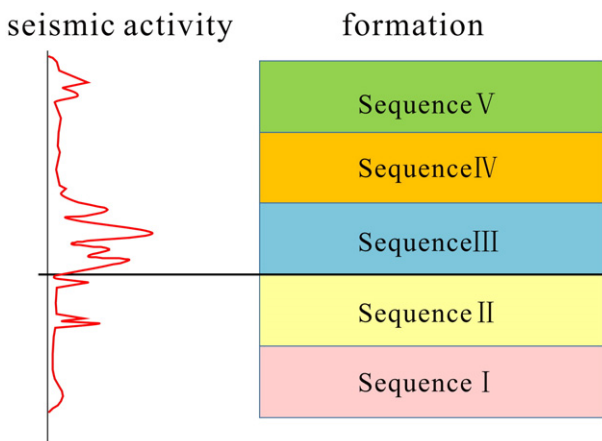


**Fig. 18.** Proposed seismic activity of the lowermost submember of Es3 in the Shahejie Formation of the Shulu Sag, east China. The seismic scale is relative, not exact.

and increase connectivity between sand bodies (Shanmugam, 2006). These sedimentary dikes could be oil stained, suggesting that they have served as conduits for fluid migration. The dark substance around calcarenous dikes in Fig. 19A and B (white arrows) may be traces of hydrocarbon migration. Oil stains can be seen with plane polarized light (Fig. 19C). Under a fluorescence microscope, the oil and gas on the edge of gravel-sized clasts show a bright yellow fluorescence (Fig. 19D). The sedimentary dikes occur in all sizes and shapes and allow both vertical and lateral fluid communication between reservoir bodies. Therefore, sedimentary dikes are important for oil-gas migration and accumulation. Hydraulic shattering has a significant effect on transporting oil or gas for the same reason.

Diapir structures are always related to liquefaction (Berra and Felletti, 2011). The lithologies that could be liquefied include saturated calcisiltite, calcarenous, or matrix-supported rudstone: all of these can be reservoirs for petroleum accumulation. Intergranular pores in calcarenous in Fig. 6C from Sequence III of well ST1H have grease

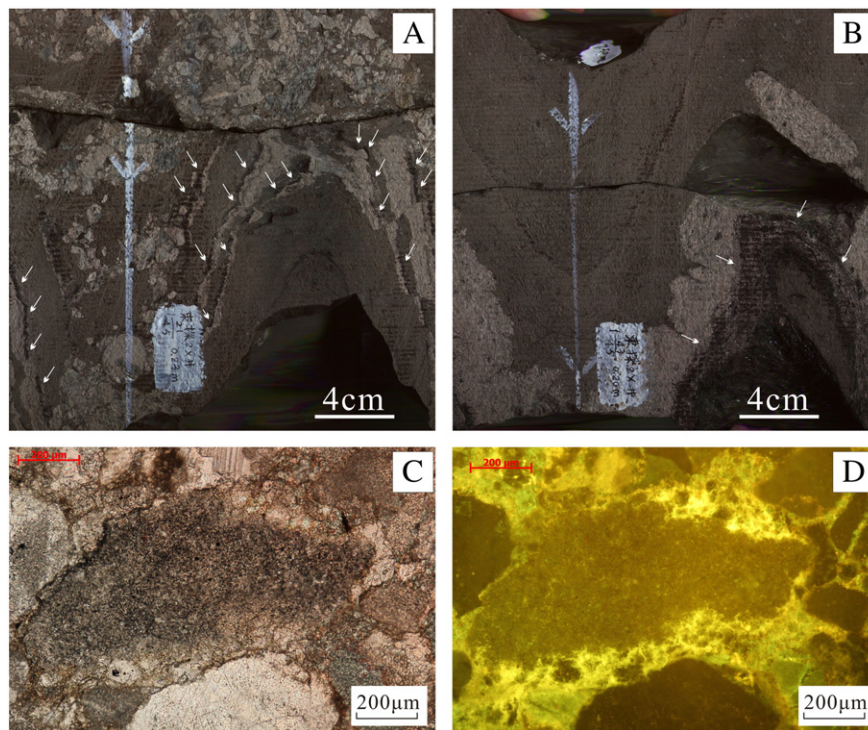


**Fig. 19.** Scanned core image and thin section of sedimentary dikes in Sequence III from the lowermost submember of Es3 of Shulu Sag. For location of wells, see Fig. 2B. (A) Calcareous dike associated with microfaults. Note the dark substance around calcarenous dikes indicated by the white arrows. From well ST2X, at 3725.17 m. (B) Calcareous dike. Note the dark substance around calcarenous dikes (the white arrows). From well ST2X, at 3729.40 m. (C)–(D) Photomicrographs of calcarenous under planar-polarized light and incident ultraviolet light, showing organic matter fluorescing yellow in intergranular pores. Same depth as B. Arrows indicate the direction of the bottom of the strata, not the top.

spots (Fig. 20A) and are yellow under a fluorescence microscope (Fig. 20B). These diapiric structures may form traps if their scale is large enough (Chapman, 1983). Similarly, calcarenous with load-flame structure can be effective reservoir rocks due to intergranular and intragranular pore space.

Loop bedding and convolute lamination are mainly made of thin interbeds of calcisiltite and calcilutite in the Shulu Sag. Fractures between the layers could act as good migration channels for the oil and gas (Fig. 20C) as confirmed by the fluorescing yellow of interlaminations within loop bedding in Fig. 20D from Sequence V of well J97.

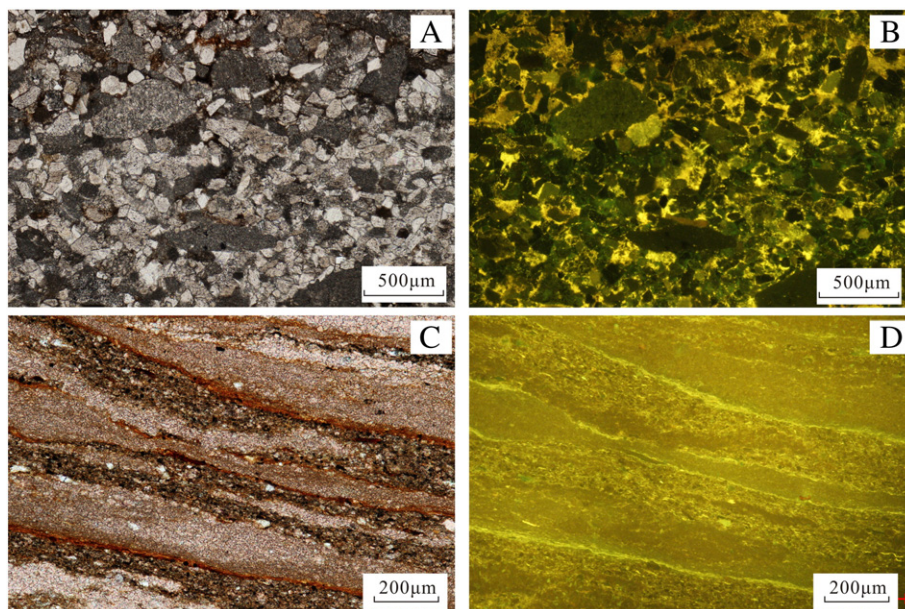


**Fig. 20.** Thin section of diapir structure and loop bedding in Sequences III and V from the lowermost submember of Es3 of the Shulu Sag. For location of wells, see Fig. 2B. (A) Photomicrograph of calcarenous in arched diapir of Fig. 6C. Planar-polarized light. From well ST1H, at 4080.1 m. (B) Same as (A) under incident ultraviolet light showing oil traces of intergranular pores fluorescing yellow. (C) Photomicrographs of loop bedding in Fig. 9C. Planar-polarized light. Note fissures between thin interbeds of calcisiltite and calcilutite. From well J97, at 3449.24 m. (D) Same as (C) under ultraviolet light showing oil trace in yellow in the interlamination of the loop bedding.

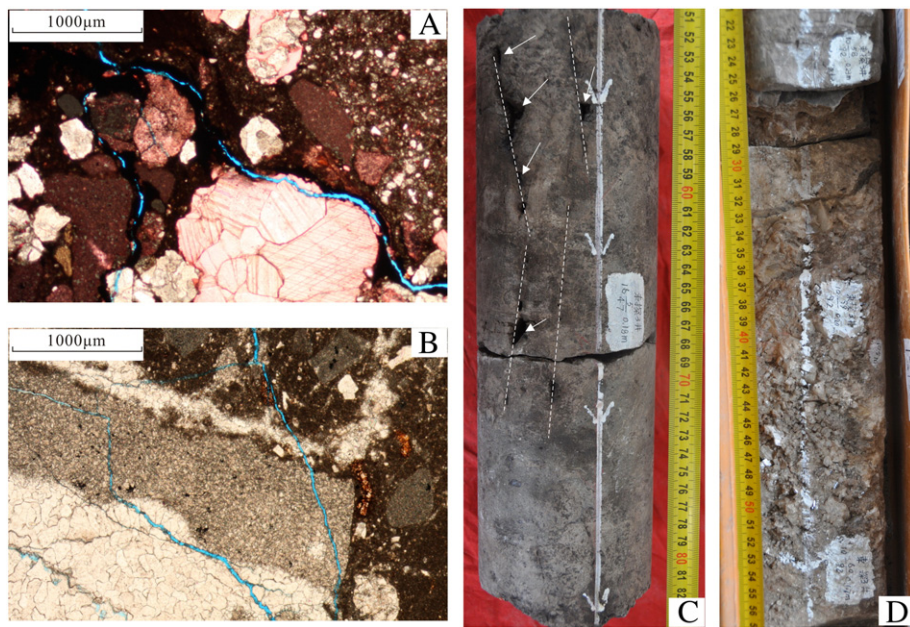


**Fig. 21.** Scanned core image and thin section showing brittle deformation in Sequences I, II, and III from the lowermost submember of Es3 of the Shulu Sag. For location of wells, see Fig. 2B. (A) Zigzag-shaped fissures (fissures are shown in blue) cutting through the gravels. Planar-polarized light. From well ST1H, at 3989.6 m. (B) Net-shaped fissures (fissures are shown in blue) across the gravels. Planar-polarized light. From well ST1H, at 4085.27 m. (C) Oil trace in the dissolution pore (white arrows) along a fracture surface from well ST3 at 4262.11 m. (D) Structural fractures filled with abundant crystallized calcite from well ST3 at 3980.13 m. Scale is in centimeters. Arrows indicate the direction of the bottom of the strata, not the top.

#### 4.4.2. Brittle deformation

Sedimentary faults and fractures induced by earthquakes can be used for oil and gas migration channels; however, they can store oil and gas as well. Zigzag-shaped microfractures can cut larger clasts and interconnect layering (Fig. 21A and B). These fractures can connect the original pores and form good network seepage fields. Although porosity was not substantially higher, permeability was increased greatly. Seismic activity not only can remold unconsolidated sediments but also can have strong effects within the consolidated sediments. Broken rock from seismic shaking may produce fractures that can connect the original pores, greatly improving reservoir performance and playing a very important role in oil and gas migration and accumulation. For example, in wells ST3 and ST1H, earthquakes produced a large number of fractures in the underlying strata (e.g., Sequence I and Sequence II) (see Table 1). These microfractures were caused clearly by later tectonic movement since they are not syndepositional faults, perhaps caused by the Xinhe or Taijiazhuang fault. Fractures are usually filled with micrite, calcite, or clay (El Taki and Pratt, 2012). According to data on fracture densities and fill, the fractures of Sequence I and Sequence II in well ST3 mostly are filled by oil, calcite, and asphalt (Table 1). Dissolution commonly develops in fractures and adjacent areas (Machel et al., 2014). Calcite cements always tend to be dissolved in the late diagenetic stage (Taylor, 1990). Hydrocarbon migration traces are still faintly visible in the dissolution pores along fracture surfaces in well ST3 (Fig. 21C). Part of the dissolution pores and pores within calcite cements can be migration channels for oil and gas (Fig. 21D).

#### 4.4.3. Seismoturbidites and mixed-source rudstone

Seismoturbidites are present in the lacustrine sublittoral to profundal zones and they are surrounded by dark calcilutite which can be source rock. The physical properties of clast-supported rudstone are better for oil-gas storage than laminated calcilutite and massive calcilutite from sublittoral to profundal lacustrine environments. Seismoturbidites are thought to be the favorable locations for oil accumulation. The injection of hydrocarbon is conducive to the preservation of primary pore space. The voids of clast-supported rudstone and matrix-supported rudstone includes intragranular pores within dissolved silexite (Fig. 22A and B) or grain limestone, intercrystalline pores (Fig. 22C and D) in the clasts of crystalline dolomite.

Mixed-source rudstones are excellent reservoirs because they have two components: Ordovician and Cambrian carbonate rocks can store hydrocarbons, and Paleogene intraclasts have a certain capacity for oil generation. The composition of gravel-sized micritic intraclasts is calcilutite with organic matter, pyrite, and small quartz grains. Total organic carbon (TOC) and the amount of hydrocarbons (S<sub>2</sub>) produced during pyrolysis are useful measurements to evaluate the generative potential of these source rocks (Alias et al., 2012; Shalaby et al., 2012). In well ST2X of Sequence III (3722–3729 m), TOC values range from 0.94 to 4.2 wt.%, with an average of 1.88 wt.%, S<sub>1</sub> from 0.46 to 2.49 mg HC/g rock, with an average of 1.37 mg HC/g rock, S<sub>2</sub> from 3.47 to 25.1 mg HC/g rock, with an average of 12.43 mg HC/g rock. According to the standard set by Zhao et al. (2014), 90% of the analyzed samples have good, very good, or excellent generative potential, with

**Table 1**

Fracture statistics based on the cores.

Well	Depth/m	Sequence	Number of fractures	Fracture density/meter	Fracture type	Composition of fillings	Fill situation
ST3	3969.64–3996.04	II	23	0.87	High-angle	Oil, calcite, and asphalt	Full
ST3	4094.85–4100.4	II	16	3.1	High-angle	Oil, calcite, and asphalt	Full
ST3	4250.26–4269.44	I	21	1.09	High-angle	Oil, calcite, and asphalt	Full
ST1H	4203.82–4213.48	II	14	1.45	High-angle	Calcite	Full

High-angle means that fracture angle is >60°.

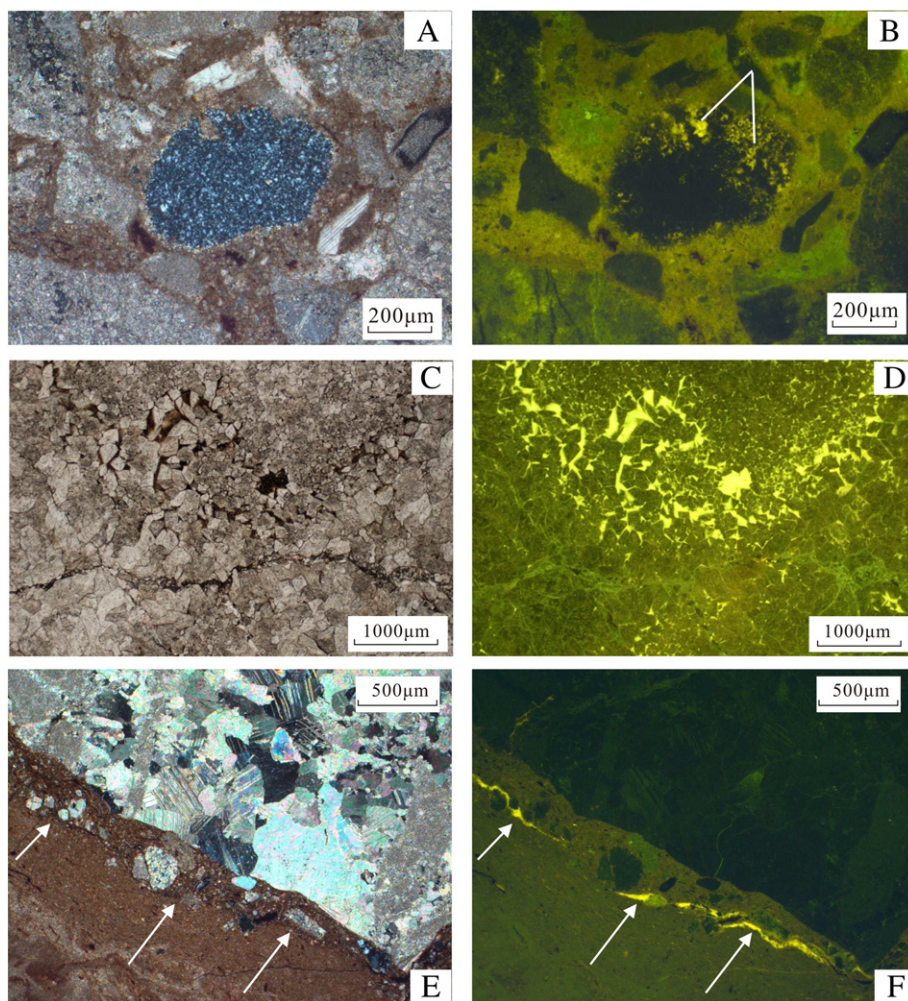


**Fig. 22.** Thin section showing reservoir spaces of seismoturbidites and mixed-source rudstone in Sequence III from the lowermost submember of Es3 of the Shulu Sag. For location of wells, see Fig. 2B. (A) Intragrannular pore within dissolved chert in center under crossed nichols. From well ST2X at 3722.32 m. (B) Same as (A) under ultraviolet light with organic matter fluorescing yellow. (C) Brown oil in intercrystal pores of dolomites. Planar-polarized light. From well ST1H, at 3979.4 m. (D) Same as (C) under ultraviolet light with oil fluorescing in a light yellow color. (E) Fissures created from diagenetic shrinkage between micritic intraclasts and matrix from well ST2X at 3725.17 m. Crossed nichols. (F) Same as (E) under ultraviolet light showing oil in fracture fluorescing yellow.

**Table 2**  
Reservoir performance of each sediment in well ST1H.

Depth/m	Lithology	Percent content of organic matter/%	Porosity/%	Permeability/ $\times 10^{-3} \mu\text{m}^2$
3959.92	Seismoturbidites	2.8	1.2	0.85
3961	Seismoturbidites	1.98	1.4	0.40
3963.6	Seismoturbidites	1.83	1.9	1.30
3966.25	Seismoturbidites	3.98	2.2	14.70
3967.4	Seismoturbidites	1.49	2.1	1.64
4082.98	Seismoturbidites	1.65	1.6	17.10
4085.52	Seismoturbidites	0.83	1.5	9.11
3971.3	Calcilitute	0	1.0	0.04
3973.52	Calcilitute	0	1.4	0.04
3977.1	Calcilitute	0	0.5	0.04
4072.43	Calcilitute	0	0.9	0.04
4077.55	Calcilitute	0	0.4	0.04
3988.85	SSDS	0.66	0.6	0.48
4080.05	SSDS	0.43	1.3	1.21
4086.6	SSDS	1.36	1.2	1.42
4073.65	Calcilitute with fissure	–	1.5	3.79

– means untested data.

Percent content of organic matter is percentage of total area of kerogen, colloid and asphalt amount observed under a fluorescence microscope.

TOC values  $> 1.0$  wt.%. The Paleozoic clasts transported from the Ningjin uplift are characterized by containing significant reservoir space for hydrocarbon accumulation. Besides intragrannular pores and intergranular pores, fissures created from diagenetic shrinkage (Fig. 22E and F) can be an important site for oil-gas accumulation. It is a result of synaeresis of micritic intraclasts under the pressure of the overlying layer in very early diagenesis (Calver and Baillie, 1990).

#### 4.4.4. Reservoir performance

Paleoseismic activity could produce many SSDSs, fractures, and slump rudstones. Clearly, SSDSs are favorable to the accumulation of oil and gas. They are always related to matrix-supported rudstone, mix-source rudstone, or calcarenites in the Shulu Sag. The improvement to reservoir quality depends on the morphology, dimension, and lithology of SSDSs. The large-scale SSDSs account for a high degree of vertical and lateral connectivity or storage capacity. If the influence of fractures is ignored, reservoir performance of layers with deformation is better than that without deformation (see Table 2). Fissures can connect nonpermeability layers and improve reservoir connectivity greatly. If the laminated calcilitute and massive calcilitute without deformation are not affected by fissures, the permeability is rather poor, only  $0.04 \times 10^{-3} \mu\text{m}^2$  (Table 2) because they only have micropores as pore space. Microfractures are important control factors for oil-gas

occurrence in the Shulu Sag. Carbonate rudstones are usually potential targets for exploration due to their primary pores and dissolved pores. The average area percent content of organic matter of seismoturbidites in ST1H can reach 2.08, while calcilutite without fissures do not emit light (Table 2).

## 5. Conclusions

Approximately 400-m-long cores from 12 wells in the Paleogene fill of the Shulu Sag contain many SSDSs and large sets of seismoturbidites. The nearby NW-trending Taijiazhuang fault and the NNE-trending Xinhe fault were clearly active during sedimentation. Sediment deformational features are widely present, especially as repeated deformed units alternating with undeformed units, and thus can be attributed to episodic seismic activity. They are interpreted as having formed by liquefaction, shear stresses, brittle deformation, or slumps. Deformation structures include sedimentary dikes, hydraulic shattering, diapir structures, convolute lamination, load-flame structures, ball-and-pillow structures, loop bedding, subsidence structures, and synsedimentary faults. Although cores lack three-dimensional perspective and lateral continuity to recognize seismically induced SSDSs, they can provide a more complete stratigraphic succession. The vertical sequence of seismites of the Shulu Sag exhibits from the base to the top, underlying undeformed layers, synsedimentary faults, liquefaction of carbonate rocks, alloigenic seismoturbidites, and overlying undeformed layers, representing a complete succession from undeformed strata to deformed strata, back to undeformed strata.

This study represents an attempt to explore the significance of paleoseismic events for hydrocarbon accumulation. Sedimentary dikes may serve as conduits for fluid migration. Calcarenite in diapiric and load-flame structures could provide effective reservoir pores. Fissures developed in unconsolidated sediment or consolidated rock can enhance permeability significantly and promote migration and accumulation of oil. Seismoturbidites are good hydrocarbon reservoirs as well. Influences on the properties of reservoir rock made by paleoearthquakes are consequently important and should be considered in oil exploration.

## Acknowledgments

We sincerely thank the extremely valuable comments from Professors Brian Pratt and Massimo Moretti that immensely helped us to clarify our manuscript objectives. The study was supported by the China National Science and Technology Major Project (2011ZX05009-002). We highly appreciate that Huabei (North China) Oil Company, CNPC provided core scanning images and other primary data. Critical and constructive comments from Professor E.H. Gierlowski-Kordesch greatly improved the manuscript.

## References

- Alfaro, P., Delgado, J., Estévez, A., Molina, J.M., Moretti, M., Soria, J.M., 2002. Liquefaction and fluidization structures in Messinian storm deposits (Bajo Segura Basin, Betic Cordillera, southern Spain). *International Journal of Earth Sciences* 91, 505–513.
- Alias, F.L., Abdullah, W.H., Hakimi, M.H., Azhar, M.H., Kugler, R.L., 2012. Organic geochemical characteristics and depositional environment of the Tertiary Tanjong Formation coals in the Pinangah area, onshore Sabah, Malaysia. *International Journal of Coal Geology* 104, 9–21.
- Allen, J.R.L., 1977. The possible mechanics of convolute lamination in graded sand beds. *Journal of the Geological Society* 134, 19–31.
- Alsop, G.I., Marco, S., 2011. Soft-sediment deformation within seismogenic slumps of the Dead Sea Basin. *Journal of Structural Geology* 33, 433–457.
- Arnaud, F., Lignier, V., Revel, M., Desmet, M., Beck, C., Pourchet, M., Charlet, F., Trentesaux, A., Tribouillard, N., 2002. Flood and earthquake disturbance of  $^{210}\text{Pb}$  geochronology (Lake Anterne, NW Alps). *Terra Nova* 14, 225–232.
- Berra, F., Pelletti, F., 2011. Syndepositional tectonics recorded by soft-sediment deformation and liquefaction structures (continental Lower Permian sediments, Southern Alps, Northern Italy): stratigraphic significance. *Sedimentary Geology* 235, 249–263.
- Bertrand, S., Charlet, F., Chapron, E., Fagel, N., De Batist, M., 2008. Reconstruction of the Holocene seismotectonic activity of the Southern Andes from seismites recorded in Lago Icalma, Chile, 39°S. *Palaeogeography, Palaeoclimatology, Palaeoecology* 259, 301–322.
- Bhattacharya, H.N., Bandyopadhyay, S., 1998. Seismites in a Proterozoic tidal succession, Singhbhum, Bihar, India. *Sedimentary Geology* 119, 239–252.
- Bowman, D., Korjenkov, A., Porat, N., 2004. Late-Pleistocene seismites from Lake Issyk-Kul, the Tien Shan range, Kyrgyzstan. *Sedimentary Geology* 163, 211–228.
- Braga, J.C., Comas, M.C., 1999. Environmental significance of an uppermost Pliocene carbonate debris flow at site 978. In: Zahn, R., Comas, M.C., Klaus, A. (Eds.), *Proceedings of the Ocean Drilling Program, Scientific Results* 161, pp. 77–81.
- Calver, C.R., Baillie, P.W., 1990. Early diagenetic concretions associated with intrastratal shrinkage cracks in an Upper Proterozoic dolomite, Tasmania, Australia. *Journal of Sedimentary Research* 60, 293–305.
- Calvo, J.P., Rodriguez-Pascua, M., Martin-Velazquez, S., Jimenez, S., Vicente, G.D., 1998. Microdeformation of lacustrine laminitic sequences from Late Miocene formations of SE Spain: an interpretation of loop bedding. *Sedimentology* 45, 279–292.
- Carrillo, E., Beck, C., Audemard, F.A., Moreno, E., Ollarves, R., 2008. Disentangling late Quaternary climatic and seismo-tectonic controls on Lake Mucubají sedimentation (Mérida Andes, Venezuela). *Palaeogeography, Palaeoclimatology, Palaeoecology* 259, 284–300.
- Chapman, R.E., 1983. *Petroleum Geology*. Elsevier, Amsterdam (415 pp.).
- Chapron, E., Beck, C., Pourchet, M., Deconinck, J.-F., 1999. 1822 earthquake-triggered homogenite in Lake Le Bourget (NW Alps). *Terra Nova* 11, 86–92.
- Doig, R., 1986. A method for determining the frequency of large magnitude earthquakes using lake sediments. *Canadian Journal of Earth Sciences* 23, 930–937.
- Doig, R., 1990. 2300 yr history of seismicity from silting events in Lake Tadoussac, Charlevoix, Quebec. *Geology* 18, 820–823.
- dos Anjos, S.M.C., De Ros, L.F., de Souza, R.S., de Assis Silva, C.M., Sombra, C.L., 2000. Depositional and diagenetic controls on the reservoir quality of Lower Cretaceous Pendência sandstones, Potiguar rift basin, Brazil. *American Association of Petroleum Geologists Bulletin* 84, 1719–1742.
- Du, Y.S., Zhang, C.H., Han, X., Gu, S.Z., Lin, W.J., 2001. Earthquake event deposits in Mesoproterozoic Kunyang Group in central Yunnan Province and its geological implications. *Science in China (Series D): Earth Sciences* 44, 600–608.
- Du, Y.S., Xu, Y.J., Yang, J.H., 2008. Soft-sediment deformation structures related to earthquake from the Devonian of the Eastern North Qilian Mts. and its tectonic significance. *Acta Geologica Sinica-English Edition* 82, 1185–1193.
- Dzulynski, S., Smith, A.J., 1963. Convolute lamination, its origin, preservation, and directional significance. *Journal of Sedimentary Research* 33, 616–627.
- El Taki, H., Pratt, B.R., 2012. Syndepositional tectonic activity in an epicontinental basin revealed by deformation of subaqueous carbonate laminites and evaporites: seismites in Red River strata (Upper Ordovician) of southern Saskatchewan, Canada. *Bulletin of Canadian Petroleum Geology* 60, 37–58.
- Ethridge, F.G., 1993. Core description. In: Morton-Thompson, Diane, Wood, Arnold (Eds.), *Development Geology Reference Manual. AAPG Methods in Exploration Series* 10, pp. 198–200.
- Ettensohn, F.R., Zhang, C.H., Gao, L.Z., Lierman, R.T., 2011. Soft-sediment deformation in epicontinental carbonates as evidence of paleoseismicity with evidence for a possible new seismogenic indicator: accordion folds. *Sedimentary Geology* 235, 222–233.
- Eyles, N., Clark, B.M., 1985. Gravity-induced soft-sediment deformation in glaciomarine sequences of the Upper Proterozoic Port Askaig Formation, Scotland. *Sedimentology* 32, 789–814.
- Ezquerro, L., Moretti, M., Liesa, C.L., Luzón, A., Simón, J.L., 2015. Seismites from a well core of palustrine deposits as a tool for reconstructing the palaeoseismic history of a fault. *Tectonophysics* 655, 191–205.
- Fanetti, D., Anselmetti, F.S., Chapron, E., Sturm, M., Vezzoli, L., 2008. Megaturbidite deposits in the Holocene basin fill of Lake Como (southern Alps, Italy). *Palaeogeography, Palaeoclimatology, Palaeoecology* 259, 323–340.
- Faridpathi, F.Y., Ergin, M., 2012. Holocene sedimentation in the tectonically active Tekirdağ Basin, western Marmara Sea, Turkey. *Quaternary International* 261, 75–90.
- Fortuin, A.R., Dabrio, C.J., 2008. Evidence for Late Messinian seismites, Nijar Basin, south-east Spain. *Sedimentology* 55, 1595–1622.
- Ghosh, S.K., Pandey, A.K., Pandey, P., Ray, Y., Sinha, S., 2012. Soft-sediment deformation structures from the Paleoproterozoic Damtha Group of Garhwal Lesser Himalaya, India. *Sedimentary Geology* 261–262, 76–89.
- Gierlowski-Kordesch, E.H., 1998. Carbonate deposition in an ephemeral siliciclastic alluvial system: Jurassic Shuttle Meadow Formation, Newark Supergroup, Hartford Basin, USA. *Palaeogeography, Palaeoclimatology, Palaeoecology* 140, 161–184.
- Gierlowski-Kordesch, E.H., 2010. Lacustrine carbonates, in carbonates in continental settings, volume 1: facies, environments, and processes. In: Alonso-Zarza, A.M., Tanner, L.H. (Eds.), *Developments in Sedimentology* 61. Elsevier, Amsterdam, pp. 1–101.
- Giles, M.R., 1987. Mass transfer and problems of secondary porosity creation in deeply buried hydrocarbon reservoirs. *Marine and Petroleum Geology* 4, 188–204.
- Goldfinger, C., 2009. Sub-aqueous paleoseismology. In: McCalpin James, I. (Ed.), *Paleoseismology*, Second Ed., pp. 119–170.
- Goldfinger, C., 2011. Submarine paleoseismology based on turbidite records. *Annual Review of Marine Science* 3, 35–66.
- Gorsline, D.S., De Diego, T., Nava-Sánchez, E.H., 2000. Seismically triggered turbidites in small margin basins: Alfonso Basin, western Gulf of California and Santa Monica Basin, California borderland. *Sedimentary Geology* 135, 21–35.
- Guiraud, M., Plaziat, J.-C., 1993. Seismites in the fluvio-deltaic Bima sandstones: identification of paleoseisms and discussion of their magnitudes in a Cretaceous synsedimentary strike-slip basin (Upper Benue, Nigeria). *Tectonophysics* 225, 493–522.
- Gutiérrez-Pastor, J., Nelson, C.H., Goldfinger, C., Escutia, C., 2013. Sedimentology of seismo-turbidites off the Cascadia and northern California active tectonic continental margins, northwest Pacific Ocean. *Marine Geology* 336, 99–119.

- He, B.Z., Qiao, X.F., Jiao, C.L., Xu, Z.Q., Cai, Z.H., Guo, X.P., Zhang, Y.L., 2014. Palaeo-earthquake events during the late Early Palaeozoic in the central Tarim Basin (NW China): evidence from deep drilling cores. *Geologos* 20, 105–123.
- Hempton, M.R., Dewey, J.F., 1983. Earthquake-induced deformational structures in young lacustrine sediments, East Anatolian Fault, southeast Turkey. *Tectonophysics* 98, T7–T14.
- Hibsch, C., Alvarado, A., Yépez, H., Perez, V.H., Sébrier, M., 1997. Holocene liquefaction and soft-sediment deformation in Quito (Ecuador): a paleoseismic history recorded in lacustrine sediments. *Journal of Geodynamics* 24, 259–280.
- Jiang, Z.X., Chen, D.Z., Qiu, L.W., Liang, H.B., Ma, J., 2007. Source-controlled carbonates in a small Eocene half-graben lake basin (Shulu Sag) in central Hebei Province, North China. *Sedimentology* 54, 265–292.
- Jones, A.P., Omosto, K., 2000. Towards establishing criteria for identifying trigger mechanisms for soft-sediment deformation: a case study of Late Pleistocene lacustrine sands and clays, Onikobe and Nakayamadaira Basins, northeastern Japan. *Sedimentology* 47, 1211–1226.
- Kahle, C.F., 2002. Seismogenic deformation structures in microbialites and mudstones, Silurian Lockport Dolomite, northwestern Ohio, U.S.A. *Journal of Sedimentary Research* 72, 201–216.
- Kong, D.Y., Shen, H., Liu, J.Y., Yin, W., 2005. Origin of the transverse accommodation zone of the Shulu subbasin in the Jizhong Depression. *Geology in China* 32, 166–171 (in Chinese with English abstract).
- Leroy, S.A.G., Schwab, M.J., Costa, P.J.M., 2010. Seismic influence on the last 1500-year infill history of Lake Sapanca (North Anatolian Fault, NW Turkey). *Tectonophysics* 486, 15–27.
- Liu, H., Jiang, Z.X., Zhang, R.F., Zhou, H.W., 2012. Gravels in the Daxing conglomerate and their effect on reservoirs in the Oligocene Langgu Depression of the Bohai Bay Basin, North China. *Marine and Petroleum Geology* 29, 192–203.
- Lowe, D.R., 1975. Water escape structures in coarse-grained sediments. *Sedimentology* 22, 157–204.
- Machel, H.G., Sumrall, J.B., Kambesis, P.N., Mylroie, J.R., Mylroie, J.E., Lace, M.J., 2014. Episodic fluid flow and dolomitization by methane-bearing pore water of marine paragenesis in an accretionary prism setting, Barbados, West Indies. *Journal of Sedimentary Research* 84, 58–71.
- Martel, A.T., Gibling, M.R., 1993. Clastic dykes of the Devon-Carboniferous Horton Bluff Formation, Nova Scotia: storm-related structures in shallow lakes. *Sedimentary Geology* 87, 103–119.
- Martín-Chivelet, J., Palma, R.M., López-Gómez, J., Kietzmann, D.A., 2011. Earthquake-induced soft-sediment deformation structures in Upper Jurassic open-marine microbialites (Neuquén Basin, Argentina). *Sedimentary Geology* 235, 210–221.
- McKee, E.D., Goldberg, M., 1969. Experiments on formation of contorted structures in mud. *Geological Society of America Bulletin* 80, 231–244.
- McLaughlin, P.I., Brett, C.E., 2004. Eustatic and tectonic control on the distribution of marine seismites: examples from the Upper Ordovician of Kentucky, USA. *Sedimentary Geology* 168, 165–192.
- Mohindra, R., Bagati, T.N., 1996. Seismically induced soft-sediment deformation structures (seismites) around Sumdo in the lower Spiti valley (Tethys Himalaya). *Sedimentary Geology* 101, 69–83.
- Molina, J.M., Alfaro, P., Moretti, M., Soria, J.M., 1998. Soft-sediment deformation structures induced by cyclic stress of storm waves in tempestites (Miocene, Guadalquivir Basin, Spain). *Terra Nova* 10, 145–150.
- Montenat, C., Barrier, P., d'Esteve, P.O., 1991. Some aspects of the recent tectonics in the Strait of Messina, Italy. *Tectonophysics* 194, 203–215.
- Montenat, C., Barrier, P., d'Esteve, P.O., Hibsch, C., 2007. Seismites: an attempt at critical analysis and classification. *Sedimentary Geology* 196, 5–30.
- Moretti, M., 2000. Soft-sediment deformation structures interpreted as seismites in middle-late Pleistocene aeolian deposits (Apulian foreland, southern Italy). *Sedimentary Geology* 135, 167–179.
- Moretti, M., Sabato, L., 2007. Recognition of trigger mechanisms for soft-sediment deformation in the Pleistocene lacustrine deposits of the Sant'Arcangelo Basin (Southern Italy): seismic shock vs. overloading. *Sedimentary Geology* 196, 31–45.
- Moretti, M., Alfaro, P., Caselles, O., Canas, J.A., 1999. Modelling seismites with a digital shaking table. *Tectonophysics* 304, 369–383.
- Moretti, M., Soria, J.M., Alfaro, P., Walsh, N., 2001. Asymmetrical soft-sediment deformation structures triggered by rapid sedimentation in turbiditic deposits (Late Miocene, Guadij Basin, Southern Spain). *Facies* 44, 283–294.
- Mugnier, J.L., Huyghe, P., Gajurel, A.P., Upreti, B.N., Jouanne, F., 2011. Seismites in the Kathmandu basin and seismic hazard in central Himalaya. *Tectonophysics* 509, 33–49.
- Mutti, E., Lucchi, F.R., Séguert, M., Zanzucchi, G., 1984. Seismoturbidites: a new group of resedimented deposits. *Marine Geology* 55, 103–116.
- Nakajima, T., Kanai, Y., 2000. Sedimentary features of seismoturbidites triggered by the 1983 and older historical earthquakes in the eastern margin of the Japan Sea. *Sedimentary Geology* 135, 1–19.
- Neuwerth, R., Suter, F., Guzman, C.A., Gorin, G.E., 2006. Soft-sediment deformation in a tectonically active area: the Plio-Pleistocene Zarzal Formation in the Cauca Valley (Western Colombia). *Sedimentary Geology* 186, 67–88.
- Nichols, R.J., Sparks, R.S.J., Wilson, C.J.N., 1994. Experimental studies of the fluidization of layered sediments and the formation of fluid escape structures. *Sedimentology* 41, 233–253.
- Obermeier, S.F., 1996. Use of liquefaction-induced features for paleoseismic analysis—an overview of how seismic liquefaction features can be distinguished from other features and how their regional distribution and properties of source sediment can be used to infer the location and strength of Holocene paleo-earthquakes. *Engineering Geology* 44, 1–76.
- Owen, G., 1987. Deformation processes in unconsolidated sands. In: Jones, M.E., Preston, R.M.F. (Eds.), *Deformation of Sediments and Sedimentary Rocks*. Geological Society Special Publication 29, pp. 11–24.
- Owen, G., 1996. Experimental soft-sediment deformation: structures formed by the liquefaction of unconsolidated sands and some ancient examples. *Sedimentology* 43, 279–293.
- Owen, G., Moretti, M., 2011. Identifying triggers for liquefaction-induced soft-sediment deformation in sands. *Sedimentary Geology* 235, 141–147.
- Owen, G., Moretti, M., Alfaro, P., 2011. Recognising triggers for soft-sediment deformation: current understanding and future directions. *Sedimentary Geology* 235, 133–140.
- Pratt, B.R., 1994. Seismites in the Mesoproterozoic Altyn Formation (Belt Supergroup), Montana: a test for tectonic control of peritidal carbonate cyclicity. *Geology* 22, 1091–1094.
- Pratt, B.R., 1998. Syneresis cracks: subaqueous shrinkage in argillaceous sediments caused by earthquake-induced dewatering. *Sedimentary Geology* 117, 1–10.
- Pratt, B.R., 2001. Oceanography, bathymetry and syndepositional tectonics of a Precambrian intracratonic basin: integrating sediments, storms, earthquakes and tsunamis in the Belt Supergroup (Helena Formation, ca. 1.45 Ga), western North America. *Sedimentary Geology* 141–142, 371–394.
- Qiao, X.F., Li, H.B., 2009. Effect of earthquake and ancient earthquake on sediments. *Journal of Palaeogeography* 11, 593–610 (in Chinese with English abstract).
- Qiao, X.F., Song, T.R., Gao, L.Z., Peng, Y., Li, H.B., Gao, M., Song, B., Zhang, Q.D., 1994. Seismic sequence in carbonate rocks by vibrational liquefaction. *Acta Geologica Sinica-English Edition* 7, 243–265.
- Qiao, X.F., Gao, L.Z., Peng, Y., 2007. Mesoproterozoic earthquake events and breakup of the Sino-Korean Plate. *Acta Geologica Sinica-English Edition* 81, 385–397.
- Qiao, X.F., Li, H.B., Qiu, Z.L., 2013. Seismites: paleo-seismic records in the sedimentary rock. In: Feng, Z.Z. (Ed.), *Sedimentology of China*, Second Ed. Petroleum Industry Press, Beijing, pp. 507–615 (in Chinese).
- Rana, N., Bhattacharya, F., Basavaiah, N., Pant, R., Juyal, N., 2013. Soft sediment deformation structures and their implications for Late Quaternary seismicity on the South Tibetan Detachment System, Central Himalaya (Uttarakhand), India. *Tectonophysics* 592, 165–174.
- Rodríguez-Pascua, M.A., Calvo, J.P., De Vicente, G., Gómez-Gras, D., 2000. Soft-sediment deformation structures interpreted as seismites in lacustrine sediments of the Prebetic Zone, SE Spain, and their potential use as indicators of earthquake magnitudes during the Late Miocene. *Sedimentary Geology* 135, 117–135.
- Rodríguez-López, J.P., Meléndez, N., Soria, A.R., Liesa, C.L., Van Loon, A.J., 2007. Lateral variability of ancient seismites related to differences in sedimentary facies (the synrift Escucha Formation, mid-Cretaceous, eastern Spain). *Sedimentary Geology* 201, 461–484.
- Rodríguez-Pascua, M.A., Garduño-Monroy, V.H., Israde-Alcántara, I., Pérez-López, R., 2010. Estimation of the paleoeepicentral area from the spatial gradient of deformation in lacustrine seismites (Tierras Blancas Basin, Mexico). *Quaternary International* 219, 66–78.
- Rossetti, D.F., Góes, A.M., 2000. Deciphering the sedimentological imprint of paleoseismic events: an example from the Aptian Codó Formation, northern Brazil. *Sedimentary Geology* 135, 137–156.
- Santos, M.G.M., Almeida, R.P., Mountney, N.P., Fragoso-Cesar, A.R.S., 2012. Seismites as a tool in the palaeoenvironmental reconstruction of fluvial deposits: the Cambrian Guarda Velha Formation, southern Brazil. *Sedimentary Geology* 277–278, 52–60.
- Scott, B., Price, S., 1988. Earthquake-induced structures in young sediments. *Tectonophysics* 147, 165–170.
- Séguret, M., Labaume, P., Madariaga, R., 1984. Eocene seismicity in the Pyrenees from megaturbidites of the South Pyrenean Basin (Spain). *Marine Geology* 55, 117–131.
- Seilacher, A., 1969. Fault-graded bed interpreted as seismites. *Sedimentology* 13, 155–159.
- Seilacher, A., 1984. Sedimentary structures tentatively attributed to seismic events. *Marine Geology* 55, 1–12.
- Selley, R.C., 1978. Concepts and methods of subsurface facies analysis: American Association of Petroleum Geologists. Continuing Education Course 858 Notes Series 9p, 82 pp.
- Shalaby, M.R., Hakimi, M.H., Abdullah, W.H., 2012. Organic geochemical characteristics and interpreted depositional environment of the Khatatba Formation, northern Western Desert, Egypt. *AAPG Bulletin* 96, 2019–2036.
- Shannugam, G., 2006. Deep-water Processes and Facies Models: Implications for Sandstone Petroleum Reservoirs. *Handbook of petroleum exploration and production* 5. Elsevier, Amsterdam, p. 476.
- Shiki, T., Kumon, F., Inouchi, Y., Kontani, Y., Sakamoto, T., Tateishi, M., Matsubara, H., Fukuyama, K., 2000. Sedimentary features of the seismo-turbidites, Lake Biwa, Japan. *Sedimentary Geology* 135, 37–50.
- Siemers, C.T., Tillman, R.W., 1981. Recommendations for the proper handling of cores and sedimentological analysis of core sequences. *SEPM Core Workshop* 2, 20–44.
- Sims, J.D., 1975. Determining earthquake recurrence intervals from deformational structures in young lacustrine sediments. *Tectonophysics* 29, 141–152.
- Singh, S., Jain, A.K., 2007. Liquefaction and fluidization of lacustrine deposits from Lahaul-Spiti and Ladakh Himalaya: geological evidences of paleoseismicity along active fault zone. *Sedimentary Geology* 196, 47–57.
- Song, T.R., 1988. A probable earthquake–tsunami sequence in Precambrian carbonate strata of Ming Tombs District, Beijing. *Chinese Science Bulletin* 33, 1121–1124.
- Song, I.S., Elphick, S.C., Odling, N., Main, I.G., Ngwenya, B.T., 2004. Hydromechanical behaviour of fine-grained calcilutite and fault gouge from the Aigion Fault Zone, Greece. *Comptes Rendus Geoscience* 336, 445–454.
- Strachan, L.J., 2002. Slump-initiated and controlled syndepositional sandstone remobilization: an example from the Namurian of County Clare, Ireland. *Sedimentology* 49, 25–41.

- Suter, F., Martínez, J.I., Vélez, M.I., 2011. Holocene soft-sediment deformation of the Santa Fe-Sopetrán Basin, northern Colombian Andes: evidence for pre-Hispanic seismic activity? *Sedimentary Geology* 235, 188–199.
- Tanner, P.W.G., 1998. Interstratal dewatering origin for polygonal patterns of sand-filled cracks: a case study from late Proterozoic metasediments of Islay, Scotland. *Sedimentology* 45, 71–89.
- Taşgin, K.C., Orhan, H., Türkmen, I., Aksoy, E., 2011. Soft-sediment deformation structures in the late Miocene Selmo Formation around Adiyaman area, Southeastern Turkey. *Sedimentary Geology* 235, 277–291.
- Taylor, T.R., 1990. The influence of calcite dissolution on reservoir porosity in Miocene sandstones, Picaroon Field, offshore Texas Gulf Coast. *Journal of Sedimentary Research* 60, 322–334.
- Törö, B., Pratt, B.R., 2015. Eocene paleoseismic record of the Green River Formation, Fossil Basin, Wyoming, U.S.A. - implications of synsedimentary deformation structures in lacustrine carbonate mudstones. *Journal of Sedimentary Research* 85, 855–884.
- Törö, B., Pratt, B.R., Renaut, R.W., 2015. Tectonically induced change in lake evolution recorded by seismites in the Eocene Green River Formation, Wyoming. *Terra Nova* 27, 218–224.
- Van Daele, M., Cnudde, V., Duyck, P., Pino, M., Urrutia, R., De Batist, M., 2014. Multidirectional, synchronously-triggered seismo-turbidites and debrites revealed by X-ray computed tomography (CT). *Sedimentology* 61, 861–880.
- Wagner, B., Reicherter, K., Daut, G., Wessels, M., Matzinger, A., Schwalb, A., Spirkovski, Z., Sanxhaku, M., 2008. The potential of Lake Ohrid for long-term palaeoenvironmental reconstructions. *Palaeogeography, Palaeoclimatology, Palaeoecology* 259, 341–356.
- Wallace, K., Eyles, N., 2015. Seismites within Ordovician–Silurian carbonates and clastics of Southern Ontario, Canada and implications for intraplate seismicity. *Sedimentary Geology* 316, 80–95.
- Wang, C.Y., Zhang, X.K., Lin, Z.Y., Li, X.Q., 1994. Characteristic of crustal structure in the Shulu fault basin and its vicinity. *Acta Seismologica Sinica* 7, 587–594.
- Yang, M.H., Liu, C.Y., Yang, B.Y., 2001. Mesozoic tectonic transformation in Jizhong (central Hebei Province) Basin and its petroleum geological implications. *Geotectonica et Metallogenesis* 25, 113–119 (in Chinese with English abstract).
- Yang, J.P., Wang, H.F., Nie, L.L., Li, Y., Zhang, Y., Li, J., 2014. Discovery and geological significance of seismites of Paleogene in Jinxian Sag, Jizhong Depression. *Acta Sedimentologica Sinica* 32, 634–642 (in Chinese with English abstract).
- Ye, D.Q., Zhong, X.C., Yao, Y.M., Yang, F., Zhang, S.B., Jiang, Z.X., Wang, Y.C., Sun, Z.C., Yang, S.Z., Zhao, X.L., Shen, H., Liang, H.D., Tang, W.S., Guan, X.T., Zhao, C.B., 1993. *Tertiary System in Petroliferous Regions of China Vol. I: Introduction*. Petroleum Industry Press, Beijing (407 pp., in Chinese).
- Yuan, J., 2004. The property and geological significance of seismites of Paleogene in Huimin sag, Shandong province. *Acta Sedimentologica Sinica* 22, 41–46 (in Chinese with English abstract).
- Yuan, J., Chen, X., Tian, H.S., 2006. Formation of loop bedding in Jiayang Sub-basin, Paleogene. *Acta Sedimentologica Sinica* 24, 666–671 (in Chinese with English abstract).
- Zhang, C.H., Wu, Z.J., Gao, L.Z., Wang, W., Tian, Y.L., Ma, C., 2007. Earthquake-induced soft-sediment deformation structures in the Mesoproterozoic Wumishan Formation, North China, and their geologic implications. *Science in China Series D: Earth Sciences* 50, 350–358.
- Zhao, X.Z., Li, Q., Jiang, Z.X., Zhang, R.F., Li, H.P., 2014. Organic geochemistry and reservoir characterization of the organic matter-rich calcilutite in the Shulu Sag, Bohai Bay Basin, North China. *Marine and Petroleum Geology* 51, 239–255.